# Discovery, Structure−Activity Relationship, and Biological Evaluation of Noninhibitory Small Molecule Chaperones of Glucocerebrosidase

Samarjit Patnaik,[†] Wei Zheng,[†] Jae H. Choi,[‡] Omid Motabar,[‡] Noel Southall,[†] Wendy Westbroek,[‡] Wendy A. Lea,[†] Arash Velayati,[‡] Ehud Goldin,[‡] Ellen Sidransky,[‡] William Leister,[†] and Juan J. Marugan*,[†]

[†]NIH Chemical Genomic Center, National Center for Advancing Translation Sciences, National Institutes of Health, 9800 Medical Center Drive, Rockville, Maryland, United States

[‡]Medical Genetics Branch, National Human Genome Research Institute, National Institutes of Health, Bethesda, Maryland 20892, United States

Ⓢ *Supporting Information*

ABSTRACT: A major challenge in the field of Gaucher disease has been the development of new therapeutic strategies including molecular chaperones. All previously described chaperones of glucocerebrosidase are enzyme inhibitors, which complicates their clinical development because their chaperone activity must be balanced against the functional inhibition of the enzyme. Using a novel high throughput screening methodology, we identified a chemical series that does not inhibit the enzyme but can still facilitate its translocation to the lysosome as measured by immunostaining of glucocerebrosidase in patient fibroblasts. These compounds provide the basis for the development of a novel approach toward small molecule treatment for patients with Gaucher disease.
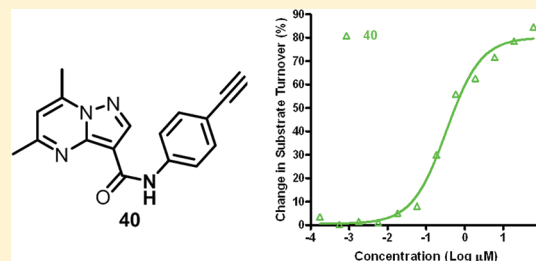
INTRODUCTION

Gaucher disease, the most common of the lipid storage disorders, results from a deficiency of the lysosomal enzyme glucocerebrosidase (GCase).[1,2] This enzyme catalyzes the hydrolysis of glucosylceramides (glucocerebrosides) (**1**, GC, Figure 1) in the lysosome. In the disease state, macrophages become engorged with GC, leading to the characteristic appearing Gaucher cell. In the most common form of Gaucher disease (type 1) clinical manifestations include enlarged spleen and liver, platelet deficiency, anemia, and bone disease. Types 2 and 3 Gaucher disease are neuronopathic forms. Patients with type 2 have a median life span of 9 months, while type 3 is more variable. Classified as a rare autosomal recessive disorder, Gaucher disease affects about 1 in every 60 000 individuals.[3] It is especially prevalent in the Ashkenazi Jewish population where the frequency is 1:800.[4]

Approved treatments for this lysosomal storage disease include enzyme replacement therapy (ERT) and substrate inhibition therapy (SRT).[5] The ERT approach involves long-term treatment via injection of a recombinant enzyme (imiglucerase) into patients with type I disease.[6] Introduced by Genzyme Therapeutics in 1994, it is quite effective in reducing and reversing the clinical symptoms of the disease. However, the treatment cost is $100000 to $400000 per year.[7] SRT is generally indicated for the treatment of adult patients with mild to moderate type I Gaucher disease for whom ERT is not a therapeutic option.[8] The prescribed drug, an iminosugar miglustat (**4**, Figure 2), developed by Actelion Pharmaceuticals inhibits glucosylceramide synthetase, reducing the production of GC in the lysosome. SRT with miglustat is often associated with side effects that include weight loss, diarrhea, tremors, and peripheral nerve damage.[9] Both ERT and SRT are ineffective against types 2 and 3 neuronopathic forms of the disease.[10]

It has been shown that in many lysosomal disorders, like Gaucher disease, the mutant enzymes often retain catalytic activity but fold improperly in the endoplasmic reticulum (ER).[11−14] This triggers ER accumulation of the mutant protein, which is eventually tagged for proteosome degradation by ubiquitination, avoiding the transport of the enzyme to the lysosome.[15,16] This mechanism has led to the proposal of an emerging form of therapy with chemical chaperones, small molecules able to bind and stabilize mutant proteins, facilitating their folding and eventually increasing their transport to the lysosome.[17−19] Improved trafficking of the mutant protein from the ER and to the lysosome results in the reduction of lysosome size and correction of the storage. Small molecule chaperones may also increase the stability of mutant enzymes toward degradation in the lysosome.[20] Ironically, most small molecule chaperones for lysosomal storage disorders reported in the literature are inhibitors of the enzyme, with the majority being iminosugars.[21] Unfortunately iminosugars have poor selectivity and exhibit a narrow therapeutic window between improving translocation and inhibiting enzyme activity.[22]

One of the first chaperone molecules reported to increase the cellular activity of GCase was N-(n-nonyl)deoxynojirimycin (NN-DNJ, **5**, Figure 2).[23] Subsequently other iminosugar inhibitors have been characterized as pharmacological
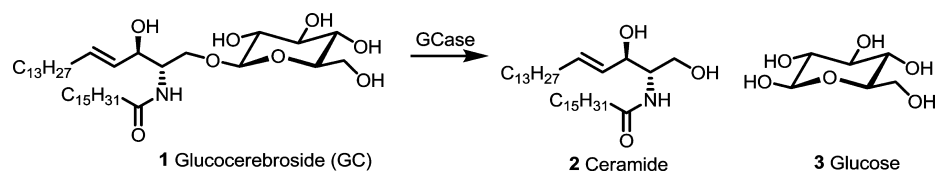
Figure 1. Chemical reaction catalyzed by glucocerebrosidase (GCase).
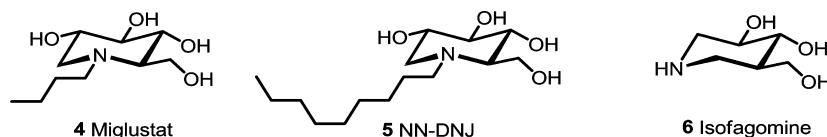

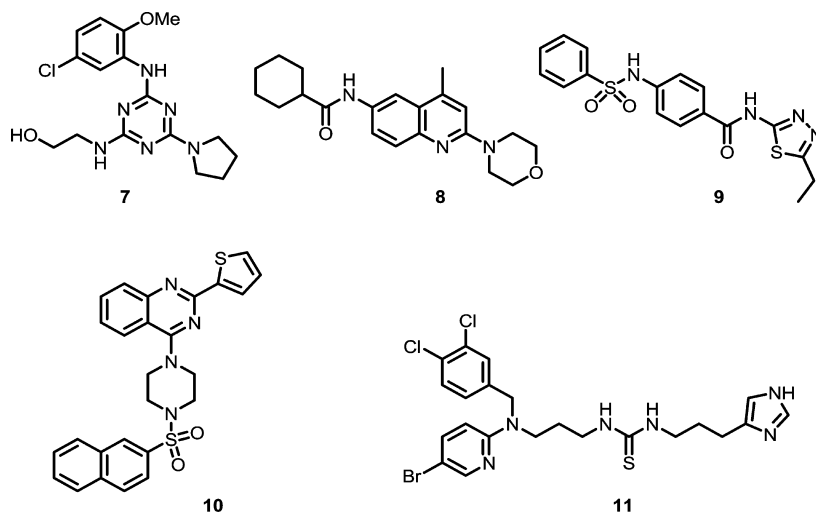**Figure 2.** Clinically relevant small molecules for Gaucher disease.

Figure 3. Representative chaperone inhibitors discovered at the NIH Chemical Genomics Center.

chaperones of GCase as well.[24−28] Out of these, isofagomine tartrate (6) has received the most attention, with Amicus Therapeutics advancing it to phase 2 clinical trials.[29] While all enrolled patients experienced an increased level of the target enzyme (GCase) in white blood cells, clinically meaningful improvements in key measures of disease were observed in just one of the 18 patients who completed the study.[30] On the basis of these results, the advancement of isofagomine was halted, thereby highlighting the difficulty of developing hydrolase inhibitors as chaperone molecules.

High throughput screens of small molecule libraries have led to the identification of novel non-iminosugar small molecule chaperones of GCase (Figure 3).[31−33] Compounds 7, 8, and 9 (Figure 3) were the first non-iminosugar GCase chaperone inhibitors disclosed by the NCGC. The primary screening assay monitored the hydrolysis of the fluorogenic substrate 4-methylumbelliferyl β-D-glucopyranoside (4MU-Glc) with purified wild type (wt) GCase. From a structural viewpoint, non-iminosugar structures have the potential advantage of reducing the risk of cross-inhibition of other glycosidases. In subsequent studies, when the GCase activity was examined with wt enzyme present in human spleen tissue homogenates, a >10-fold shift in activity was observed. In fact, inhibitors 7 and 9 were completely inactive against the N370S variant of the enzyme in spleen extracts from a Gaucher patient. This was a highly relevant observation, as the N370S mutation is the most common mutation observed in Gaucher patients.[2] The chaperone activity of inhibitors 7 and 9 was demonstrated via

a translocation assay (vide infra) in fibroblasts derived from normal tissue and patients. However, the potency in this assay was 100−1000 weaker compared to the wt enzymatic activity. Such differences in activity spurred the development of a novel high throughput assay that used spleen homogenates from patients with the N370S/N370S genotype. The new screening paradigm did not use a disease relevant mutant, but now the enzyme also operated in the presence of natural activators present in the spleen. This approach led to the discovery of non-iminosugar GCase inhibitors represented by 10 and 11 (Figure 3).[34] While compound 10 displayed potent inhibition of the enzyme derived from tissue extracts, there was a substantial loss of potency in the purified enzyme with complete inactivity against the N370S mutant (Table 1).[35] On the other hand, the chemical series represented by 11 demonstrated enzyme inhibition in all four assays represented in Table 1.[36] Compounds 10 and 11 displayed comparable chaperone activity to isofagomine at 1 and 10 μM, respectively. Interestingly, isofagomine, a more potent inhibitor of GCase (IC$_{50}$ = 30 nM), shows chaperone activity at micromolar concentrations in advanced translocation assays. On other hand, the enantiomeric L-isomer of isofagomine is the first example of a noncompetitive inhibitor of GCase (K_i = 5.7 μM) that shows chaperoning activity in patient fibroblasts causing a 1.6-fold increase in specific activity at 500 μM.[37] These facts highlight the difficulty of extrapolating results from activity-based screening assays to the actual therapeutic potential for the treatment of lysosomal storage disorders.

Table 1. Inhibitory Profile of GCase Chaperone Inhibitors Illustrated in Figure 3[a]

compd	purified GCase IC$_{50}$, μM		spleen homogenate IC$_{50}$, μM	
	wt	N370S	wt	N370S
7	0.40	11	7.9	inactive
8	0.03	0.56	2.2	3.2−12.6*
9	0.10	1.6	3.2	inactive
10	8.9	inactive	0.28	0.33
11	0.71	2.5	0.36	0.58

[a]The data represent inhibition of turnover of 4-methylumbelliferyl β-D-glucopyranoside (4MU-Glc) except where indicated with an asterisk (∗), where resorufin β-D-glucopyranoside is the substrate.

A potential reason for the discrepancy in activity observed in assays using the purified enzyme versus the spleen homogenate could be the presence of additional activating factors in the tissue. For instance, while in cells GCase activity is modulated through the binding of the allosteric activators such as saposin C,[38,39] the addition of the bile salt sodium taurocholate is required to activate the enzyme in the purified enzyme assay.[40] Therefore, the variation in inhibitory activity could be due to differences in binding with the active GCase conformation induced by detergent versus that induced by saposin C. These conformational differences could also explain why a chemical series with the capacity to activate the enzyme has not yet been identified via conventional screening assays using isolated enzyme. In fact, the amount of sodium taurocholate added to the assay is optimized to achieve a maximum signal, and therefore, further activation by a small molecule cannot be observed. In contrast, the tissue homogenate conditions do not require the addition of activating components because natural activators like saposin C are already present in the homogenate. Moreover, the V_{max} of the N370S mutant enzyme is lower than that of the wt enzyme.[41] These advantages with the new N370S spleen homogenate screening conditions have led to the discovery of a series of pyrazolo[1,5-a]pyrimidine-3-carbox-amides that displayed GCase activation at micromolar concentrations.[42]
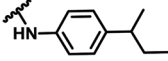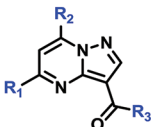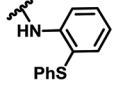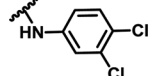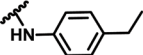
The development of GCase activators, especially in the context of chaperone therapy, is ideal because this could lead to small molecules that not only facilitate the translocation of mutant GCase to the lysosome but also increase its specific activity.[43] However, at the outset, it is important to realize that specific activators of hydrolases are most likely allosteric binders, as it is not possible to increase the rate of hydrolysis by competing for the active site with the substrate. The binding affinity of such activators and their influence on the hydrolytic reaction may vary with different GCase conformations that present themselves as the enzyme accommodates various substrates and cofactors present under different assay conditions. Additionally, the capacity of a molecule to modulate the hydrolytic function of an enzyme does not necessarily correlate with its capacity to bind, induce, and accelerate folding into a particular conformation that improves protein translocation. Therefore, modulators of enzymatic hydrolysis may not demonstrate chaperone capacity and vice versa. At the same time, if a particular chemical series shows both enzymatic modulation and the capacity to increase translocation, we expect that compounds showing greater enzymatic modulation (inhibitors or activators) will also exhibit improved translocation capacity. This follows since increments in the AC$_{50}$ imply higher affinity toward the enzyme, which often correlates with greater refolding capacity. This rationale was used to drive the SAR using the activity in the functional hydrolysis assay as a surrogate measure of affinity toward the enzyme. Subsequently, more labor-intensive translocation assays with patient fibroblasts were performed on select compounds to confirm chaperone behavior. The following account details the use of such a strategy to progress the aforementioned set of pyrazolopyrimidine activators and their development as the first publicly disclosed noninhibitory small molecule chaperones of GCase. The discussion includes a detailed description of the SAR, characterization of optimized compounds in orthogonal assays, and preliminary evaluation of pharmacokinetic properties.

■ RESULTS AND DISCUSSION

A total of 326 770 compounds were screened using the qHTS format in titrations from 90 nM to 57 μM final concentration using spleen homogenate from a Gaucher patient with genotype N370S/N370S.[44,45] From this primary screen, we identified several series of compounds that modulated the turnover of the 4MU-Glc substrate. Several iminosugar molecules, such as isofagomine, previously reported to inhibit GCase, were also found, validating the tissue homogenate

Table 2. GCase Activation Profile with 4MU-Glc as Substrate under Spleen Homogenate and Purified Enzyme Conditions[a]

Compd#	R$_1$	R$_2$	R$_3$	Spleen Homogenate N370S AC$_{50}$ μM	Spleen Homogenate wt AC$_{50}$ μM	Purified Enzyme N370S AC$_{50}$ μM	Purified Enzyme wt AC$_{50}$ μM
12	CH$_3$	CHF$_2$		2.51	3.16	14.1	12.6
13		CHF$_2$		4.60	4.61	16.3	32
14	CH$_3$	CH$_3$		3.66	4.47	15.9	14.1
15	CH$_3$	CHF$_2$		2.24	2.81	12.6	14.1

[a]Values are average of N = 2.

Scheme 1. Analogue Synthesis
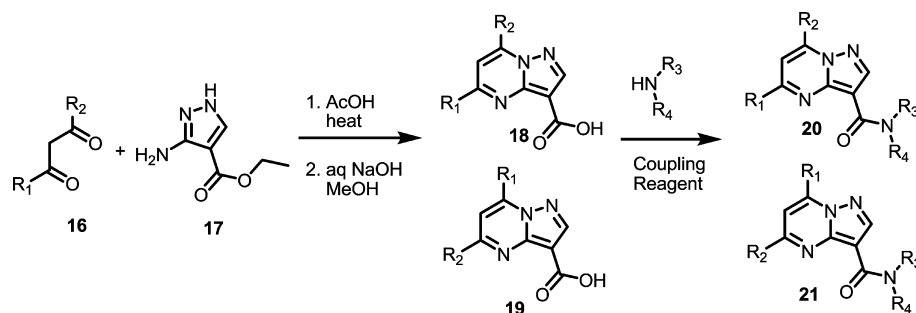
approach. Further confirmatory efforts, including the ordering of additional analogues, identified a set of pyrazolopyrimidines as activators from the screen (Table 2). Additional studies revealed that the activity in assays using N370S mutant or wild type spleen homogenate preparations (Table 2) was 3- to 10-fold better than purified enzyme conditions. Assays using resorufin β-D-glucopyranoside as the substrate failed to show consistent activation among lead molecules of this series, underscoring the importance of proper substrate choice for assay development and SAR within a particular chemical series.[46] These pyrazolopyrimidines were inactive in the absence of GCase as well as against α-glucosidase (EC 3.2.1.20) and α-galactosidase (EC 3.2.1.22) in assays following the turnover of the corresponding 4-MU-α-glucose and 4-MU-α-galactose substrates (data not shown), confirming selectivity for GCase.

This discovery of these selective GCase activators prompted the synthesis of additional analogues in order to improve activity and to evaluate the key structural features present within the chemotype critical for activity. The synthetic sequence (Scheme 1) used to generate the analogues started with the condensation of a 1,3-diketone **16** with ethyl 3-amino-1H-pyrazole-4-carboxylate **17** in acetic acid.[47,48] Initial efforts to simplify the evaluation of the amide SAR centered on the use of acetylacetone as the diketone to eliminate the formation of regioisomers ($R_1 = R_2 = CH_3$). With unsymmetrical ketones, a mixture of regioisomers (**18**, **19**) was formed, which were typically separated by chromatography. Then ester hydrolysis provided an acid that was coupled with amines or anilines to generate compounds (**20**, **21**, Scheme 1) for biological analysis.

Medicinal chemistry efforts with $R_1 = R_2 = CH_3$ led to the production of the compounds presented in Table 3. The subsequent activity tables enumerate the SAR observed toward an increase in the hydrolysis of 4MU-Glc. The SAR and activity observed with spleen homogenates derived from controls or patients with genotype N370S/N370S were comparable, and thus, for brevity, the N370S data are presented here.

Compounds derived from the coupling of 5,7-dimethyl-pyrazolo[1,5-a]pyrimidine-3-carboxylic acid (**18** or **19** with $R_1 = R_2 = CH_3$, Scheme 1) with primary aliphatic amines like methyl-, isobutyl-, or isopropylamine and pyrrolidine proved to be inactive (**22**–**25**, Table 3). However, the cyclohexylamide **26** had an AC_{50} of 10 μM, which was further improved upon the addition of a 4-tert-butyl group to the cyclohexyl core as in **27**. The other isomer **28** derived from 4-tert-butylcyclohexamine (the cis and trans forms have not been determined yet) was 2.5-fold less active. While arylmethylamides **29** and **30** were not that active, the amide derived from simple aniline **31** had an AC_{50} of 8.2 μM. Thus, it appeared that the presence of a six-membered cyclic aliphatic moiety at R_3 was critical for the
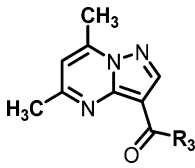
activation of GCase. The N-phenyl derivative **31** prompted an exploration of substitutions around the phenyl ring.

A simple methyl group at the para position (**32**) led to a 5-fold improvement in activity compared to the plain phenyl derivative, while a moderate improvement was noticed at the meta position (**34**). The o-methyl substitution led to loss of activity in **33** and in the 2,4-dimethylated compound **36** as well. The 3,4-dimethylated compound **35**, as well as its cyclic indane variant **37**, showed reasonable activity, underscoring the presence of an aliphatic substituent at the para position of the phenyl ring. This was further substantiated with **38** and **39**, which had AC_{50} of 3.3 and 2.3 μM with p-ethyl and tert-butyl groups, respectively. However, submicromolar activity was achieved by **40** with a terminal alkyne at the para position. The correlation of para substitution and better activity was seen with the inductively electron withdrawing aliphatic trifluoromethyl (**41**), bromo (**43**), and chloro (**44**) groups. However, a simple pyridyl ring (**46**) showed complete lack of activity. The same trend was seen with the electron withdrawing methylsulfone (**47**), cyano (**48**, **49**), methyl ketone (**50**, **51**), and acetamido (**52**, **53**) containing congeners at 3- and/or 4- positions.

The electron donating methoxy group at the para position resulted in compound **54** with an AC_{50} of 8.2 μM. However, the presence of an additional methoxy at one (**56**) or both meta positions (**55**) led to inactive compounds. Dioxolane **57** and dioxane **58**, which have conformational constraints, had similar activities compared to the p-methoxy compound **54**, implying that the freely rotating m-methoxy group present in **56** was deleterious toward activity. In conjunction with the p-methoxy group, the presence of a m-fluoro (**59**) or m-chloro atom (**60**) led to improved potencies of 1.46 and 2.06 μM, respectively.

As the SAR of the amide was being explored, a parallel approach was taken to evaluate the substitutions at the 5 (R_1) and 7 (R_2) positions of the pyrazolo[1,5-a]pyrimidine core using the chemistry described above (Scheme 1). A phenyl group at R_2 was not tolerated, while a methyl group was. This was seen consistently in the context of four different substituted phenyl amides when compared to compounds with $R_1 = R_2 = CH_3$ (**32**/**62**, **54**/**63**, **44**/**64**, **66**/**68**, Tables 4 and 5). However, the regioisomers with $R_1 = Ph$ and $R_2 = CH_3$ retained activity as observed with the 3,4-dichloro **65**, indane**70**, and 4-ethyl **73** derivatives. The replacement of the R_1 methyl with a cyclopropyl group led to compounds with almost equal potency (**13**, **67**, **69**, and **71**). Similarly, the R_2 methyl could be replaced with di- (**13**, **69**, **71**, and **72**) or trifluoromethyl (**67**) substituents to produce equipotent compounds. This SAR is well suited to ameliorate P450 mediated hepatic metabolism of the R_2 CH_3 if it becomes an issue during future in vivo studies.
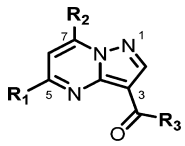
Table 3. GCase Activation of the Glycolysis of 4MU-Glc in Homogenate Derived from the Spleen of Patients with the N370S Mutation: Evaluation of the R$_3$ Group[a]

#	R$_3$	AC$_{50}$ (μM)	#	R$_3$	AC$_{50}$ (μM)
22	N-Me amide	inactive	42	3-CF$_3$-phenyl	41.1
23	isobutyl	32.6	43	4-Br-phenyl	2.06
24	isopropyl	inactive	44	3,4-dichlorophenyl	3.66
25	pyrrolidinyl	inactive	45	3,5-dichlorophenyl	25.9
26	cyclohexyl	10.3	46	pyridyl	inactive
27[a]	trans-4-tBu-cyclohexyl	4.11	47	methylsulfonylphenyl	inactive
28[a]	4-tBu-cyclohexyl (N-Me)	25.9	48	4-CN-phenyl	20.6
29	benzyl	51.7	49	3-CN-phenyl	inactive
30	furfuryl	51.7	50	4-acetylphenyl	163
31	phenyl	8.19	51	3-acetylphenyl	32.6
32	4-methylphenyl	1.63	52	4-acetamidophenyl	inactive
33	2-methylphenyl	16.3	53	3-acetamidophenyl	inactive
34	3-methylphenyl	6.51	54	4-methoxyphenyl	8.19
35	3,4-dimethylphenyl	1.46	55	3,4,5-trimethoxyphenyl	inactive
36	2,4-dimethylphenyl	13.0	56	3,4-dimethoxyphenyl	inactive
37	indanyl	2.59	57	methylenedioxyphenyl	6.51
38	4-ethylphenyl	3.26	58	ethylenedioxyphenyl	10.3
39	4-tBu-phenyl	2.31	59	methoxy-fluorophenyl	1.46
40	4-ethynylphenyl	0.36	60	methoxy-chlorophenyl	2.06
41	CF$_3$-phenyl	1.46	61	hydroxybutyl	inactive

[a]AC$_{50}$ values are average of N = 2. The assignment of relative stereochemistry of the 4-tert-butylcyclohexanamide is tentative and deduced from the ^{1}H NMR spectra of the individual racemic compounds (see Supporting Information for additional details).

Table 4. GCase Activation of the Glycolysis of 4MU-Glc in Homogenate Derived from the Spleen of Patients with the N370S Mutation: Evaluation of the R$_1$ and R$_2$ Groups[a]
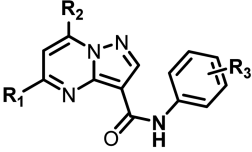

#	R$_1$	R$_2$	R$_3$	AC$_{50}$ μM
32	CH$_3$	CH$_3$	4-methylphenyl	1.63
62	CH$_3$	Ph		inactive
54	CH$_3$	CH$_3$	4-methoxyphenyl	8.19
63	CH$_3$	Ph		inactive
44	CH$_3$	CH$_3$	3,4-dichlorophenyl	3.66
64	CH$_3$	Ph		inactive
65	Ph	CH$_3$		4.36
66	CH$_3$	CH$_3$	2-(phenylthio)phenyl	18.3
13	cyclopropyl	CHF$_2$		4.60
67	cyclopropyl	CF$_3$		14.1
68	CH$_3$	Ph		inactive
37	CH$_3$	CH$_3$	indanyl	2.59
69	cyclopropyl	CHF$_2$		3.98
70	Ph	CH$_3$		8.19
26	CH$_3$	CH$_3$	cyclohexyl	10.3
71	cyclopropyl	CHF$_2$		12.6
38	CH$_3$	CH$_3$	4-ethylphenyl	3.26
72	CH$_3$	CHF$_2$		2.24
73	Ph	CH$_3$		12.9

[a]AC$_{50}$ values are average of N = 2.

As noted in the data in Tables 2−4, the nature of enzyme activation in the newly discovered activator series was demonstrated by measuring the fluorescence of 4-methyl-umbelliferone (4MU) released during the hydrolysis of 4MU-Glc (labeled as HTS in Figure 5 and Figure 4a) . In order to dispel any notion that the chemical series may be a fluorescent artifact, it was imperative to demonstrate the activation by an alternative technique. To that end, an assay was developed to measure the release of 4-MU by high performance liquid chromatography−mass spectrometry (labeled as HPLC in Figure 5).[49] Four representative active molecules from this chemical series (Table 5) were analyzed using this assay, and all exhibited a dose-dependent activation of substrate turnover. Thus, the capacity of this series to increase the turnover of the 4MU-Glc substrate was established by two separate methods. However, unlike the inhibitor isofagomine (Table 5,

Table 5. GCase Activation with Representative Pyrazolopyrimidines and Inhibition with Isofagomine in Homogenates from a N370S/N370S Genotype Gaucher Patient Spleen[a]

	Compd#	R_1	R_2	R_3	4MU-β-Glu N370S Spleen HTS AC_{50}	4MU-β-Glu N370S Spleen HPLC AC_{50}	Fluorescent Ceramide N370S Spleen HPLC AC_{50}
	40	CH_3	CH_3	$p-C\equiv CH$	0.4 μM	3.7 μM	inactive
	41	CH_3	CH_3	$p-CF_3$	1.5 μM	1.3 μM	inactive
	43	CH_3	CH_3	$p-Br$	2.1 μM	1.2 μM	inactive
	13	(cyclopropyl)	CHF_2	$o-SPh$	4.6 μM	3.0 μM	inactive
	Isofagomine				30 nM	19 nM	2.7 μM

[a]Activation was measured by monitoring the (a) fluorescence of 4MU released on hydrolysis of 4MU-Glc, (b) release of 4MU from 4MU-Glc with HPLC and (c) release of C12-BODIPY-Cer from fluorescent C12-BODIPY-GlcCer with HPLC. AC_{50} values are average of $N = 2$.
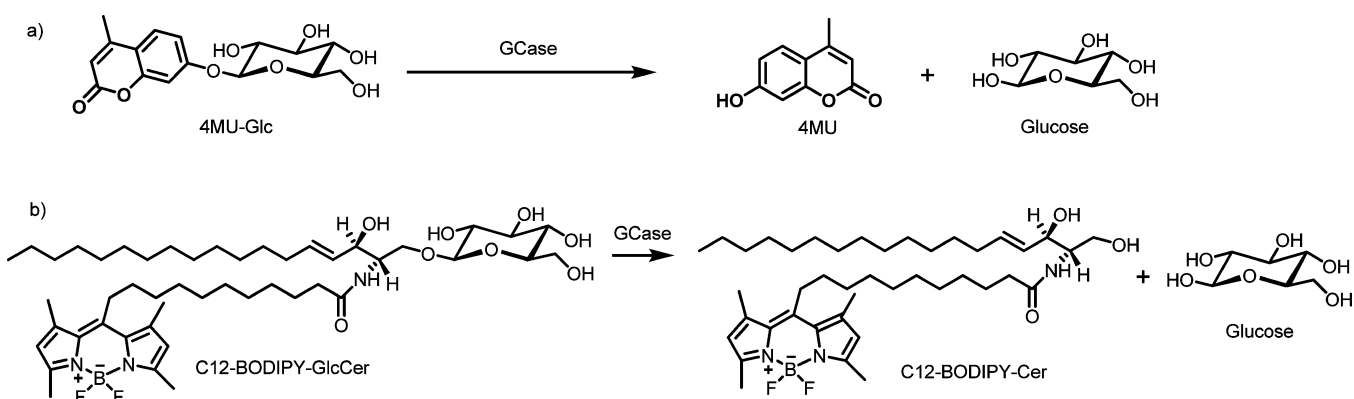

Figure 4. Two GCase assays. (a) "Blue" GCase assay. The profluorescent substrate 4MU-Glc is hydrolyzed to form glucose and 4MU (excitation peak at 365 nm; emission peak at 440 nm). This assay was used for the primary screen and can be followed by HPLC/MS. (b) "Fluorescent ceramide" GCase assay. The glucosyl ceramide fluorescent substrate (C12-BODIPY-GlcCer) is hydrolyzed to form glucose and C12-BODIPY-Cer (excitation peak at 506 nm; emission peak at 540 nm), and their ratio was detected upon separation by HPLC.
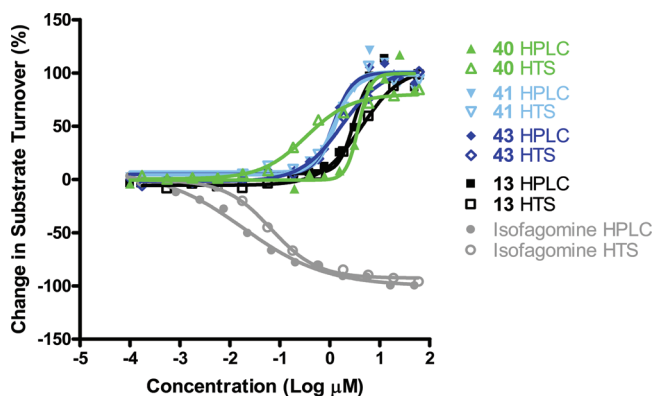

Figure 5. Concentration response profiles for **40**, **41**, **43**, **66**, and isofagomine for the assays a and b indicated in the footnote of Table 5.

$IC_{50} = 2.7$ μM), these compounds did not show an increase in substrate turnover in the analogous HPLC assay with the fluorescent glucosylceramide-like C12-BODIPY-GlcCer substrate (Figure 4b), suggesting that compounds from this series may not activate the hydrolysis of the natural substrate.

The disparate behavior toward activation of the 4MU-Glc and not the fluorescent ceramide substrate necessitated an evaluation of chaperone activity. The capacity of compounds to

increase the translocation of GCase to the lysosome was evaluated by laser scanning confocal microscopy.[50,51] Dermal fibroblasts derived from a Gaucher patient with genotype N370S/N370S were incubated for 6 days with compound **40**, or with closely related congeners at three different concentrations (1, 5, 25 μM), and the known chaperone isofagomine. After treatment, cells were fixed and stained with a custom-made GCase antibody labeled with Alexa555 (Figures 6 and 7, red), an antibody for the lysosomal marker LAMP-2 labeled with Alexa488 (Figures 6 and 7, green), and a DAPI stain for visualization of the nucleus (Figures 6 and 7, blue). In cell-based translocation assays, compounds able to enhance GCase trafficking from the ER to the lysosome should increase the overall GCase amount in the lysosomes, which will result in increased colocalization between GCase and the lysosomal marker. In this study DMSO, which was the vehicle (Figure 6A), and isofagomine (Figure 6B) were used as negative and positive controls. Compound **40** increased the amount of GCase protein, as evident by the brighter red color (parts C and D of Figure 6, upper left quadrant) compared to DMSO vehicle treatment (Figure 6A). Also, the increase in the intensity of the bright yellow color (parts C and D of Figure 6, lower right quadrant) indicated that the amount of GCase protein (red) was increased in the lysosomes (green) after treatment with compound **40**. Furthermore, cells incubated
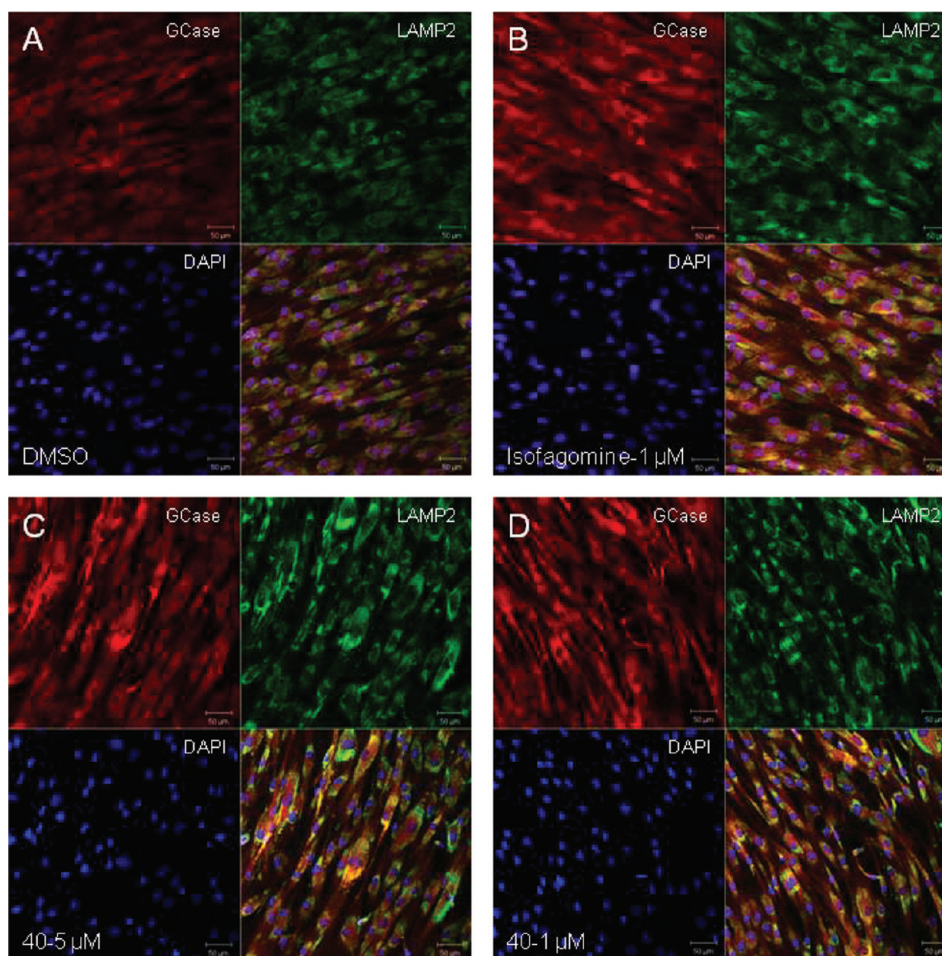
Figure 6. Translocation studies of endogenous N370S GCase enzyme in Gaucher N370S/N370S dermal fibroblasts. Fibroblasts were treated for 6 days with (A) DMSO, (B) 1 μM isofagomine, (C) 5 μM **40**, (D) 1 μM **40**. Cells were stained for LAMP-2 (green), GCase (red), and the nucleus (DAPI, blue). The bottom right quadrant in each image is an overlay of all stains; bright yellow (overlap of red and green) indicates increased GCase in the lysosome. All laser settings were held constant across all of the fields imaged. Scale bar shows 50 μm.
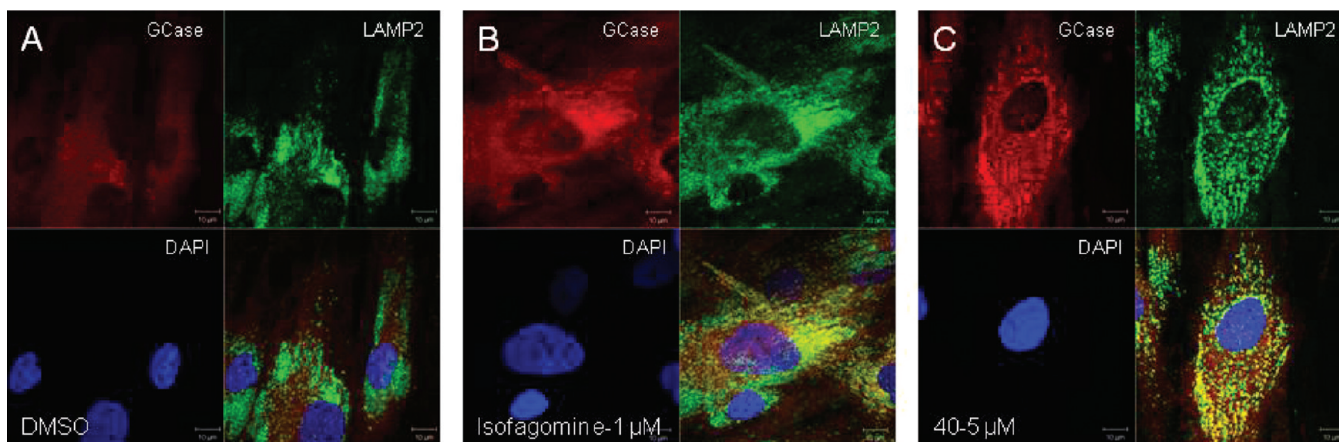

Figure 7. Translocation activity of compound **40** (C), isofagomine (B), and DMSO vehicle control (A) in N370S/N370S Gaucher fibroblasts. The red, green, and blue stains represent GCase, the lysosomal marker LAMP2, and nucleus (DAPI), receptively. All laser settings were constant across all of the fields imaged. Shown are high magnification images with scale bar indicating 10 μm.

with 1 μM isofagomine (Figure 6B) or compound **40** (parts C and D of Figure 6) resulted in increased amounts GCase in the lysosome compared to DMSO vehicle treatment, confirming that the positive control worked in our assay (Figure 6A). The high magnification images of treatment with compound **40**

(Figure 7C, yellow, bottom right quadrant) clearly showed the presence of CGase (red) in lysosomes (green), even in the periphery of the cell.

The translocation experiment proved that our chemical series exemplified by the pyrazolopyrimidine **40** was able to increase

levels of GCase in N370S/N370S patient fibroblasts. Whether this translated to an increase in specific activity was yet to be verified. To that end we incubated **40** with fibroblasts derived from four different cell lines (control, N370S carrier, N370S/N370S, L444P/L444P) and measured GCase activity after 6 days (Figure 8). Gratifyingly, irrespective of genotype, an
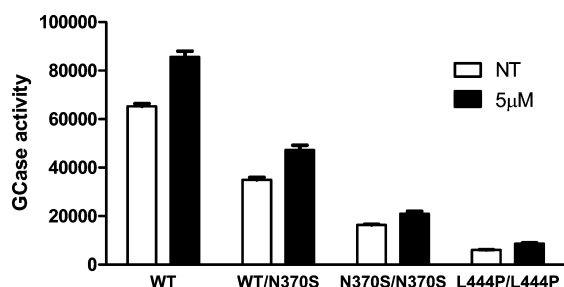

Figure 8. GCase activity, as measured by hydrolysis of 4MU-Glc, after 6 days of treatment with 5 μM **40** or no compound (NT = no treatment) in four fibroblast cell lines (WT = control, WT/370S = carrier mutation, N370S/N370S = derived from patients homozygous for N370S mutation, L444P/L444P = derived from patients homozygous for L444P mutation).

increase in activity was observed at 5 μM across all lines compared to control (NT = no treatment) without any evidence of toxicity. The compound's effect on the L444P/L444P line is significant, as this missense mutation is commonly found in the neuronopathic forms of the disease.[52] This increase in activity was not observed with the inactive control **22** (data not shown).

Microscale thermophoresis (MST), a recently developed technology that measures molecule movements under a controlled temperature gradient, was applied to determine if the putative activator series physically interacts with GCase.[53] MST uses fluorescently labeled protein targets that, on binding to ligands, can show changes in the movement of the protein molecule along the temperature gradient. This technique was best suited for binding analysis because of its low protein requirements and its sensitivity, which is critical as these allosteric activators had AC$_{50}$ values in the micromolar range in the functional assay.[54] Figure 9 shows binding affinity data with
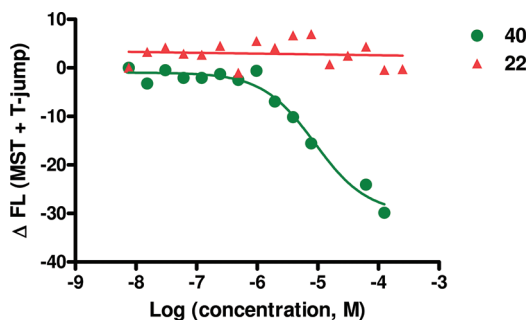

Figure 9. Change in fluorescence observed with **40** (K_d = 8.91 μM) and an inactive analogue **22** with increasing concentration in a microscale thermophoresis experiment.

GCase for the potent activator **40** and an inactive analogue **22**. In this experiment, **40** binds to fluorescently labeled GCase in a dose-dependent manner, with an apparent K_d of ~9 μM. This binding response has been recapitulated upon multiple testing. This study was performed with isolated enzyme where the series exhibited lower potency compared to the tissue

homogenate conditions. In contrast, the negative control **22** failed to display significant binding within the same titration range.
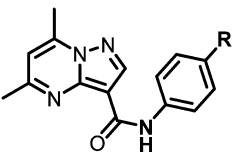
By use of these novel GCase noninhibitor chaperones, ADME studies were performed for the selection of possible candidates for in vivo studies. The stability of representative compounds from this chemical series was examined in mouse liver microsomes. As observed in Table 6, compound **40** and the closely related *p*-trifluoro compound **41** displayed good stability. The permeability of the most potent compound **40** was also analyzed in a standard Caco-2 permeability assay. The A to B and B to A apparent permeability were determined as 6.0 and 2.0 (10^{-6} cm s^{-1}). The values of these numbers below 10×10^{-6} cm s^{-1} reflect possible limitations in solubility. The efflux ratio of 0.3 suggests that the compound is not recognized by the ABC transporters expressed in the Caco-2 monolayer and therefore is expected to have reasonable good oral absorption and perhaps penetration through the blood−brain barrier, which is especially relevant for the treatment of types 2 and 3 Gaucher disease.

Following the encouraging potency and in vitro ADME properties for compound **40**, a mouse PK study was initiated. A 50 mpk ip single administration of **40** in male mice resulted in a C_{max} of 1.03 μM in plasma and a half-life of 19.3 h (Table 7, Figure 10). The total exposure in liver, which is characteristically enlarged in type 1 Gaucher disease, was quite high (>200 times higher than plasma). The compound crossed the blood−brain barrier and had ~3 times the exposure observed in the plasma. Thus, **40** appeared to reach the target organs affected in all three forms of Gaucher disease, rendering it an ideal lead molecule for preliminary in vivo proof-of-principle studies.

■ CONCLUSIONS

The use of spleen homogenate for HTS followed by medicinal chemistry optimization identified the lead pyrazolopyrimidine **40**, which displayed GCase activation by hydrolyzing 4MU-β-Glc at submicromolar AC$_{50}$ concentrations. Compound **40** also demonstrated GCase activation of purified wt and N370S enzyme with AC$_{50}$ of 5.2 and 6.5 μM, respectively, a 10-fold attenuation in potency consistent with the data in Table 2, likely due to the absence of necessary cofactors present in the spleen homogenate. While the activation of GCase with **40** and other congeners was also observed in an orthogonal HPLC assay, the series was inactive toward the hydrolysis of a fluorescent ceramide-like substrate in the same assay. In addition, these compounds failed to show GCase activation in the primary fluorescence assay with resorufin β-D-glucopyranoside as the substrate. Previously, we have observed such discrepancies in the activation of a glycolytic enzyme toward the hydrolysis of different substrates.[55] The enzyme kinetics of the hydrolysis and the outcome of the reaction depend on the reaction substrate as well as the assay conditions (for example, isolated enzyme or tissue homogenate). Thus, a compound may activate the hydrolysis of two different substrates with different efficiencies because the substrate binding is different in each case, and the compound might stabilize one particular conformation more than the other. Ongoing studies are evaluating the addition of saposin C, an allosteric activator for GCase, to assays where specific chemical series fail to show inhibition or activation.[30] The hydrolysis assay still remains a useful surrogate assay for developing SAR. The pyrazolopyrimides series demonstrated activity by increasing the translocation of GCase to the lysosome in wild

Table 6. Stability of Representative Compounds at 1 μM in Mouse Liver Microsomes after 60 min[a]

#	R	% remaining after 60 min *with NADPH*	% remaining after 60 min *without NADPH*
40	ξ—C≡CH	45	42
41	ξ—CF$_3$	83	100
43	ξ—Br	12	86

[a]The data represent the percentage of parent compound remaining.

Table 7. PK Parameters for 40 Determined in Plasma, Brain, and Liver after a 50 mpk ip Dose in Male C57BL/6 Mice

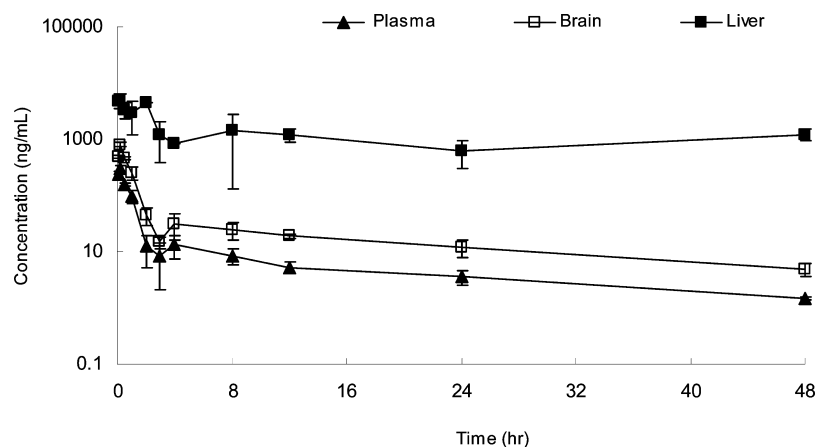| PK parameter	unit	plasma	brain	liver
T_{max}	h	0.250	0.250	0.250
C_{max}	ng/mL	298	802	5020
		(1.03 μM)	(2.76 μM)	(17.29 μM)
$T_{1/2}$	h	19.3	18.2	28.9
AUC_{last}	h·ng/mL	434	1260	54300
AUC_{INF}	h·ng/mL	474	1390	105000
$AUC_{tissue}/AUC_{plasma}$	%		290	12512

Figure 10. Mean concentration−time profiles for **40** in plasma, brain, and liver after 50 mpk ip dose in male C57BL/6 mice ($N = 3$).

type (not shown) and patient fibroblasts, with **40** exhibiting chaperone activity very similar to isofagomine at 1 μM. The chaperone activity increased in a dose-dependent manner and was not observed with a structurally related congener (**61**) that was inactive in the primary assay (not shown). Furthermore, this increase in translocation was mirrored by a consistent increase in GCase activity in fibroblasts derived from four different cell lines that included the N370S/N370S and L444P/L444P genotypes derived from Gaucher patients. Preliminary binding experiments revealed association of the compound with the wt enzyme. **40** also displayed promising pharmacokinetic properties.

The class of pyrazolpyrimidines described in this report demonstrated biochemical activation of CGase, as well as chaperone activity. These first-in-class noninhibitory chaperones have the unique advantage over existing chaperones of not being inhibitors of the GCase enzyme, and therefore, they do not need to be displaced by the natural substrate in the lysosome for the resumption of catalytic activity. These molecules are promising new candidates for chaperone therapy toward Gaucher disease and are currently being evaluated with the aim of advancing toward clinical development.

■ MATERIALS AND METHODS

Biology. The recombinant wild-type enzyme imiglucerase (Cerezyme) was obtained from Genzyme Corporation (Cambridge, MA). N370S recombinant glucocerebrosidase was a gift from Dr. Tim Edmunds at Genzyme. Spleen samples were obtained during splenectomies with informed consent under an NIH-IRB approved clinical protocol. Control spleens were obtained under an NIH protocol. 4-Methylumbelliferyl-β-D-glucopyranoside (4MU-Glc), a blue fluorogenic substrate, resorufin β-D-glucopyranoside (Res-glc), a red fluorogenic substrate, sodium taurocholate, and the buffer components were purchased from Sigma-Aldrich (St. Louis, MO). Isofagomine and N-nonyldeoxynojirimycin (NN-DNJ) were purchased from Toronto Research Biochemicals (Ontario, Canada).

The human spleen tissue was homogenized using a food blender at the maximal speed for 5 min, followed by 10 passes in a motor-driven 50 mL glass-Teflon homogenizer. The homogenate was centrifuged at 1000g for 10 min. The supernatant was then filtered using a 40 μm filter, and aliquots of resultant spleen homogenate were frozen at −80 °C until use.

Enzyme Assay in 1536-Well Plate Format. In black 1536-well plates, a BioRAPTR FRD Microfluidic workstation (Beckman Coulter, Inc., Fullerton, CA) was used to dispense 2 μL/well spleen homogenate (27 μg final) or pure enzyme solution (5 nM final) into 1536-well plates. The assay buffer for the spleen homogenate was

50 mM citric acid, 115 mM K_2HPO_4, 110 mM KCl, 10 mM NaCl, 1 mM $MgCl_2$, and 0.01% Tween-20 at pH 5. The buffer for the purified enzyme was 50 mM citric acid, KH_2PO_4 (titrated to pH 5.9 for recombinant wt enzyme and pH 7 for N370S variant), and 0.01% Tween-20. An automated pin-tool station (Kalypsys, San Diego, CA) was used to transfer 23 nL/well compound (the final titration was 0.5 nM to 58 μM) to the assay plate. After 5 min of incubation at room temperature, the enzyme reaction was initiated by the addition of 2 μL/well substrate. Final concentrations of the blue substrate (4MU-Glc) and red substrate (Res-Glc) were 1 mM and 15 μM, respectively. After 30−45 min of incubation at 37 °C, the reaction was terminated by the addition of 2 μL/well stop solution (1 M NaOH and 1 M glycine mixture, pH 10). Then 1 M Tris-HCl at pH 8.0 was used as the stop solution for the red substrate assay. The fluorescence was then measured in the Viewlux, a CCD-based plate reader (Perkin-Elmer, Waltham, MA), with Ex = 365 nm and Em = 440 nm for the blue substrate (4MU) and Ex = 573 nm and Em = 610 nm for the red substrate (resorufin).

LC−MS Hydrolysis Experiment. This assay uses liquid chromatography linked to a mass spectrometer to assess the ability of glucocerebrosidase in the spleen homogenate to cleave the profluorescent substrate 4MU-Glc or C12-BODIPY-GlcCer. Chromatography was performed using an Agilent HPLC instrument on stopped enzymatic reactions. The Agilent 1200 LC instrument was equipped with a quaternary pump, a G1315 diode array detector, and a G1321 fluorescent detector. A 4.6 mm × 250 mm Agilent Eclipse Plus C18 (5 μm) instrument at ambient temperature was used at a flow rate of 1.8 mL/min with a gradient of 85/15 (methanol/0.1% formic acid in water) to 100% methanol over 10 min. Compounds were monitored using fluorescence detection with Ex = 365 nm and Em = 440 nm for 4MU or Ex = 506 nm and Em = 540 nm for C12-BODIPY. We verified that the mass of the fluorescent peaks matched the expected ones for the substrate and product of the reaction. The concentrations of the compounds used were from 0 to 20 nM to 50 μM (1:2 dilutions from 50 μM, 9 concentrations). 140 μg/well of spleen homogenate was used. Final concentrations of 2 mM for the 4-MU-Glc and 25 μM for C12-BODIPY-Cer were used. The assay conditions were the same as the enzyme assay.

Thermophoresis Assay. Glucocerebrosidase (GC, Protalix) was labeled with a NT-647 dye (NanoTemper Technologies) and was used in the thermophoresis experiment at a final concentration of ~20 nM. A 16-point dilution series was made for selected compounds in DMSO. Each compound dilution series was subsequently transferred to protein solutions in 50 mM phosphate buffer, pH 7.2, 0.05% Tween-20. After a 15-min incubation of the labeled GC with each dilution point (1:1 mix) at room temperature, samples were filled into standard capillaries (NanoTemper Technologies). Measurements were taken on a Monolith NT.115 microscale thermophoresis system (NanoTemper) under a setting of 50% LED and 50% IR laser. Laser-on time was set at 30 s, and laser-off time was set at 5 s.

Immunocytochemistry and Laser Scanning Confocal Microscopy. Primary dermal fibroblasts derived from skin biopsies from previously described N370S/N370S Gaucher patients were seeded in Lab-Tek 4 chamber slides (Fisher Scientific, Pittsburgh, PA). After compound treatment, fibroblasts were fixed in 3% paraformaldehyde. The cells were permeabelized with 0.1% Triton-X for 10 min and blocked in PBS containing 0.1% saponin, 100 μM glycine, 0.1% BSA, and 2% donkey serum followed by incubation with mouse monoclonal LAMP-2 (1:100, Developmental Studies Hybridoma Bank, University of Iowa, Iowa City, IA) and the rabbit polyclonal anti-GCase R386 antibody (1:500). The cells were washed and incubated with secondary donkey anti-mouse or anti-rabbit antibodies conjugated to ALEXA-488 or ALEXA-555, respectively (Invitrogen, Carlsbad, CA), washed again, and mounted in VectaShield with DAPI (Vector Laboratories, Burlingame, CA).

Cells were imaged with a Zeiss 510 META confocal laser-scanning microscope (Carl Zeiss, Microimaging Inc., Germany) using an argon (458, 477, 488, 514 nm) 30 mW laser, a HeNe (543 nm) 1 mW laser, and a laser diode (405 nm). Low and high magnification images were acquired using a Plan-Apochromat 20×/0.75 objective and a Plan-Apochromat 100×/1.4 oil DIC objective, respectively. Images were taken with the same laser settings.

Cellular Assay To Measure GCase Specific Activity. Fibroblast cell lines from controls, carriers, and Gaucher individuals (N370S, L444P) were seeded in 96-well clear-bottom blank plates with a density of 5000 cells/well in DMDM containing 15% FBS and GlutaMax. After 1 day the medium is changed to OPTI-MEM containing 5% FBS and no antibiotics. Each compound is dissolved in the same medium to desired concentrations (1−20 μM final), and the cells were treated with compound for 6 days. The plates were assayed on day 6 by adding 1 volume of 0.2 M acetate buffer, pH 4, and 1 volume of PBS, pH 7.4, containing 2.5 mM 4MU-Glc. Plates were incubated at 37 °C for 1 h. The reaction was stopped by adding 1 M glycine and 1 M NaOH, which lyzed the cells. The fluorescence was measured by a plate reader at (Em = 355, Ex = 460). The second set of luminescence plates containing the same lines was used for viability assay using CellTiter-Glo (Promega) as described by the manufacturer.

Microsome Stability. The test agent is incubated in duplicate with CD-1 mouse liver microsomes at 37 °C. The mixture contains microsomal protein in 100 mM potassium phosphate, 2 mM NADPH, 3 mM $MgCl_2$, pH 7.4. A control is run for each test agent omitting NADPH to detect NADPH-free degradation. At indicated times, an aliquot is removed from each experimental and control mixture and mixed with an equal volume of ice-cold stop solution (0.3% AcOH in MeCN containing haloperidol, diclofenac, or other internal standard). Stopped mixtures are incubated at least 10 min at −20 °C, and an additional volume of water is added. The samples are centrifuged to remove precipitated protein, and the supernatants are analyzed by LC−MS/MS to quantitate the remaining parent. Data are reported as percent remaining by dividing by the time zero concentration value.

Caco-2 Permeability. Caco-2 cells grown in tissue culture flasks are trypsinized, suspended in medium, and the suspensions were applied to wells of a collagen-coated BioCoat cell environment in 24-well format (BD Biosciences) at 24 500 cells per well. The cells are allowed to grow and differentiate for 3 weeks, feeding at 2-day intervals. To verify that Caco-2 cell monolayers are properly formed, aliquots of the cell buffers are analyzed by fluorescence to determine the transport of the impermeable dye Lucifer yellow. For permeability, the test agent is added to the apical (A) or basolateral (B) side and amount of permeation to the other side is determined by LC−MS/MS. The A-side buffer contains 100 μM Lucifer yellow dye in transport buffer (1.98 g/L glucose in 10 mM HEPES, 1× Hank's balanced salt solution), pH 6.5, and the B-side buffer is transport buffer, pH 7.4. Caco-2 cells are incubated with these buffers for 2 h. Data are expressed as permeability (P_{app}), where dQ/dt is the rate of permeation. In bidirectional permeability studies, the asymmetry index (AI) or efflux ratio is also calculated. AI > 1 indicates a potential substrate for PGP or other active transport.

Pharmacokinetics. C57BL/6 mice, 18−26 g, male, N = 36, were purchased from SLAC Laboratory Animal Co. Ltd. The animals had free access to food and water. The ip dosing solution was prepared in 20% PEG 400 + 80% (20% HP-β-CD). Brain and liver samples were homogenized with 3 volumes of PBS (pH 7.4) before sample extraction. The final concentration was adjusted with a dilution factor of 4, assuming 1 g of wet brain equals 1 mL. LC−MS/MS analysis of samples was done with an Acquity UPLC BEH C18 column, flow rate 0.6 mL/min, with a mobile phase consisting of solvent A (H_2O−0.2% FA, 10 mM NH_4OAC), solvent B (MeOH−0.2%FA, 10 mM NH_4OAC). No clinical findings were observed during the entire life study.

Chemistry. General Methods. All solvents and reagents were purchased from Sigma Aldrich and other commercial vendors and used as such. Purification was done with either normal phase SiO_2 chromatography using Biotage purification stations or reverse phase chromatography on a Waters semipreparative HPLC column. High resolution mass spectrometry data were recorded on an Agilent 6210 time-of-flight LC−MS system. Confirmation of molecular formula was accomplished using electrospray ionization in the positive mode with the Agilent Masshunter software (version B.02). ^{1}H and ^{13}C NMR

spectra were recorded on a Varian Inova 400 MHz spectrometer. Chemical shifts are reported in δ with the solvent resonance as the internal standard (DMSO-d_6 δ 2.50 for ^{1}H, DMSO-d_6 δ 39.5 for ^{13}C).

Analytical purity analysis and retention times reported here were performed using three methods. Method 1 involves the following: column, Phenomenex Luna C18 (3 μm, 3 mm × 75 mm); run time, 8 min; gradient, 4−100% acetonitrile in water over 7 min; mobile phase, acetonitrile (0.025% TFA), water (0.05% TFA); flow rate, 1 mL/min; temperature, 50 °C; UV wavelength, 220 and 254 nm.

Method 2 involves the following: detection UV, 214 nm; Gemini column; solvent A, water; solvent B, 90% acetonitrile, 10% water, 0.1% AcOH modifier; gradient initial condition, 100% A with hold time 0.5 min; gradient time, 3 min; gradient final concentration, 100% B; gradient final hold, 0.5 min; run time, 5 min; flow rate, 1.5 mL/min.

Method 3 involves the following: detection UV, 220 nm; Phenomenex Luna 2.5 μm C18 100 mm × 2.00 mm column; solvent A, water (0.05% TFA); solvent B, acetonitrile (0.025% TFA); gradient initial condition, 95% A, 5% B with hold time 0.1 min; gradient time, 2.1 min; gradient final concentration, 100% B, 5% A; gradient final hold, 0.5 min and then another hold for further 0.3 min with 98% A, 2% B; run time, 3 min.; flow rate, 0.30−0.5 mL/min.

All analogues were determined to have >95% purity based on the above methods.

General Procedure toward Analogues.
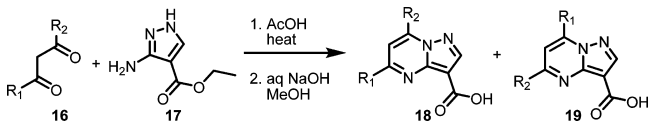
Step 1 ($R_1 = R_2 = Me$). Pentane-2,4-dione (1.46 mL, 14.2 mmol) and ethyl 3-amino-1H-pyrazole-4-carboxylate (2.00 g, 12.9 mmol) were heated in a sealed tube with acetic acid (10 mL) at 110 °C overnight. The reaction reached completion by LC−MS (t_R = 3.08 min). The acetic acid was removed by blowing air on the mixture overnight. (For $R_1 \neq R_2$, at this stage the residue was purified by flash SiO$_2$ chromatography to separate the regioisomers **18** and **19**. Each was separately taken to the next step.) The crude residue of ethyl 5,7-dimethylpyrazolo[1,5-a]pyrimidine-3-carboxylate (assumed to be 12.89 mmol) was suspended in MeOH (15 mL) and treated with 7.2 M sodium hydroxide (5.37 mL, 38.7 mmol). The mixture was heated to 80 °C (at this temperature the solid dissolved) and then stirred for 3 h. The mixture was cooled and neutralized to pH 6−7. The slurry was filtered via a Büchner funnel under house vacuum, and the solid residue was washed with water and then diethyl ether to obtain 5,7-dimethylpyrazolo[1,5-a]pyrimidine-3-carboxylic acid (1.4 g, 7.3 mmol, 57% yield). LC−MS (method 3): t_R = 2.61 min. ^{1}H NMR (400 MHz, DMSO-d_6) δ ppm 2.57 (s, 3 H), 2.71 (s, 3 H), 7.10 (s, 1 H), 8.50 (s, 1 H). ^{13}C NMR (101 MHz, DMSO-d_6, 100 °C) δ ppm 16.0, 23.9, 106.0, 109.2, 145.8, 146.3, 146.6, 160.3, 164.4.
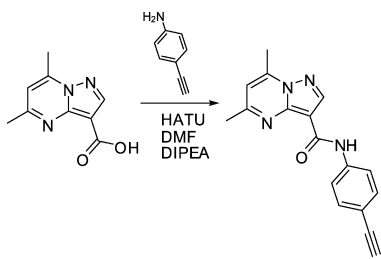
Step 2. 5,7-Dimethylpyrazolo[1,5-a]pyrimidine-3-carboxylic acid (722 mg, 3.78 mmol), 4-ethynylaniline (442 mg, 3.78 mmol), and HATU (1436 mg, 3.78 mmol) were taken up in DMF (10 mL) and then treated with diisopropylethylamine (1.979 mL, 11.33 mmol). The contents were stirred at room temperature overnight. The product had precipitated from reaction mixture. The mixture was diluted with water and filtered through a Büchner funnel under house vacuum. The residue was washed with water (×2), then CH$_2$Cl$_2$, diethyl ether, and air-dried to obtain N-(4-ethynylphenyl)-5,7-dimethylpyrazolo[1,5-a]-pyrimidine-3-carboxamide (500 mg, 1.72 mmol, 46% yield). LC−MS (method 3): t_R = 3.65 min. ^{1}H NMR (400 MHz, DMSO-d_6) δ ppm

2.71 (s, 3 H), 2.77 (s, 3 H), 4.11 (s, 1 H), 7.21 (s, 1 H), 7.49 (d, J = 8.6 Hz, 2 H), 7.77 (d, J = 8.6 Hz, 2 H), 8.65 (s, 1 H), 10.31 (s, 1 H). ^{13}C NMR (101 MHz, DMSO-d_6, 100 °C) δ ppm 15.6, 23.7, 78.6, 83.1, 103.5, 109.9, 115.9, 118.6, 131.9, 138.9, 144.7, 144.8, 147.0, 159.2, 161.4.

This coupling procedure was used to synthesize all analogues. Analogues were obtained with >95% purity by simple filtration/washing/drying and/or by preparative purification on a Waters semipreparative HPLC. The column used was a Phenomenex Luna C18 (5 μm, 30 mm × 75 mm), and the flow rate was 45 mL/min. The mobile phase consisted of acetonitrile and water (each containing 0.1% trifluoroacetic acid). Generally a gradient of 10−50% acetonitrile over 8 min was used during the purification. The fraction collection was triggered by UV detection (220 nm, 254 nm).

For R_1 = Me, R_2 = Ph, and R_1 = Ph, R_2 = Me. Step 1 from the above general procedure was followed with 1-phenylbutane-1,3-dione (1.05 g, 6.45 mmol), ethyl 3-amino-1H-pyrazole-4-carboxylate (1.00 g, 6.45 mmol), and acetic acid (15 mL). Flash SiO$_2$ column chromatography (10−80% EtOAc/hexanes) provided ethyl 7-methyl-5-phenylpyrazolo[1,5-a]pyrimidine-3-carboxylate (0.23 g, 0.82 mmol, 13% yield). LC−MS (method 2): t_R = 3.66 min. ^{1}H NMR (400 MHz, DMSO-d_6) δ ppm 1.37 (t, J = 7.0 Hz, 3 H), 2.84 (s, 3 H), 4.32 (q, J = 7.2 Hz, 2 H), 7.60 (m, 3 H), 7.94 (s, 1 H), 8.32 (m, 2 H), 8.63 (s, 1 H). Ethyl 5-methyl-7-phenylpyrazolo[1,5-a]pyrimidine-3-carboxylate was also provided (0.95 g, 3.4 mmol, 52% yield). LC−MS (method 2): t_R = 3.56 min. ^{1}H NMR (400 MHz, DMSO-d_6) δ ppm 1.33 (t, J = 7.0 Hz, 3 H), 2.68 (s, 3 H), 4.31 (q, J = 7.0 Hz, 2 H), 7.40 (s, 1 H), 7.62 (m, 3 H), 8.06 (m, 2 H), 8.57 (s, 1 H). The separated pure esters were hydrolyzed to the corresponding acids (characterization data below).

5-Methyl-7-phenylpyrazolo[1,5-a]pyrimidine-3-carboxylic Acid (Precursor to 62, 63, 64, 68. LC−MS (method 2): t_R = 3.11 min. ^{1}H NMR (400 MHz, DMSO-d_6) δ ppm 2.65 (s, 3 H), 7.34 (s, 1 H), 7.51−7.66 (m, 3 H), 8.04 (d, J = 6.7 Hz, 2 H), 8.52 (s, 1 H) (note: acid O$\underline{H}$ is not visible). ^{13}C NMR (101 MHz, DMSO-d_6) δ ppm 24.5, 101.8, 110.4, 128.4, 129.6, 130.1, 131.1, 146.0, 147.0, 148.0, 162.6, 163.3.

7-Methyl-5-phenylpyrazolo[1,5-a]pyrimidine-3-carboxylic Acid (Precursor to 65, 70, 73). LC−MS (method 2): t_R = 3.13 min. ^{1}H NMR (400 MHz, DMSO-d_6) δ ppm 2.82 (s, 3 H), 7.54−7.63 (m, 3 H), 7.86 (s, 1 H), 8.24−8.31 (m, 2 H), 8.58 (s, 1 H), 12.32 (br s, 1 H). ^{13}C NMR (101 MHz, DMSO-d_6) δ ppm 17.0, 102.6, 106.6, 127.5, 129.0, 131.0, 136.2, 147.2, 147.5, 147.8, 157.4, 163.3.

5-Cyclopropyl-7-(difluoromethyl)pyrazolo[1,5-a]pyrimidine-3-carboxylic Acid (Precursor to 13, 69, 71) and 5-Cyclopropyl-7-(trifluoromethyl)pyrazolo[1,5-a]pyrimidine-3-carboxylic Acid (Precursor to 67). The title compounds were purchased from Chembridge and used directly in coupling reactions.

Analytical Data for Compounds. 22. ^{1}H NMR (400 MHz, DMSO-d_6) δ ppm 2.62 (s, 3 H), 2.73 (s, 3 H), 2.89 (d, J = 4.7 Hz, 3 H), 7.10 (s, 1 H), 7.95 (q, J = 4.7 Hz, 1 H), 8.48 (s, 1 H). LC−MS (method 1): t_R = 3.71 min. HRMS (m/z) calcd for C$_{10}$H$_{13}$N$_4$O (M + H)$^+$ 205.1084, found 205.1085

23. ^{1}H NMR (400 MHz, DMSO-d_6) δ ppm 0.95 (m, 6 H), 1.83 (m, 1 H), 2.61 (s, 3 H), 2.74 (s, 3 H), 3.22 (t, J = 6.3 Hz, 2 H), 7.12 (s, 1 H), 8.15 (t, J = 6.1 Hz, 1 H), 8.48 (s, 1 H). LC−MS (method 1): t_R = 5.08 min. HRMS (m/z) calcd for C$_{13}$H$_{19}$N$_4$O (M + H)$^+$ 247.1553, found 247.1559

24. ^{1}H NMR (400 MHz, DMSO-d_6) δ ppm 1.22 (m, 6 H), 2.61 (s, 3 H), 2.73 (s, 3 H), 4.09 (m, 1 H), 7.10 (s, 1 H), 7.91 (d, J = 7.8 Hz, 1 H), 8.47 (s, 1 H). LC−MS (method 1): t_R = 4.66 min. HRMS (m/z) calcd for C$_{12}$H$_{17}$N$_4$O (M + H)$^+$ 233.1397, found 233.1397

25. LC−MS (method 1): t_R = 3.84 min. HRMS (m/z) calcd for C$_{13}$H$_{17}$N$_4$O (M + H)$^+$ 245.1397, found 245.1399

26. ^{1}H NMR (400 MHz, DMSO-d_6) δ ppm 1.35 (m, 5 H), 1.56 (m, 1 H), 1.70 (m, 2 H), 1.87 (m, 2 H), 2.61 (s, 3 H), 2.73 (s, 3 H), 3.87 (m, 1 H), 7.11 (s, 1 H), 8.08 (d, J = 7.8 Hz, 1 H), 8.48 (s, 1 H). LC−MS (method 1): t_R = 5.55 min. HRMS (m/z) calcd for C$_{15}$H$_{21}$N$_4$O (M + H)$^+$ 273.1710, found 273.1713.

27. [1H] NMR (400 MHz, DMSO-d_6) δ ppm 0.88 (m, 9 H), 1.12 (m, 5 H), 1.77 (m, 2 H), 2.05 (m, 2 H), 2.61 (m, 3 H), 2.73 (m, 3 H), 3.72 (m, 1 H), 7.11 (m, 1 H), 7.92 (d, J = 7.7 Hz, 1 H), 8.47 (m, 1 H). LC−MS (method 1): t_R = 6.94 min. HRMS (m/z) calcd for $C_{19}H_{29}N_4O$ (M + H)$^+$ 329.2336, found 329.2342.

28. [1H] NMR (400 MHz, DMSO-d_6) δ ppm 0.89 (s, 9 H), 1.27 (m, 3 H), 1.56 (m, 2 H), 1.68 (m, 2 H), 1.81 (m, 2 H), 2.60 (s, 3 H), 2.74 (s, 3 H), 4.26 (m, 1 H), 7.13 (m, 1 H), 8.46 (m, 2 H). LC−MS (method 1): t_R = 6.82 min. HRMS (m/z) calcd for $C_{19}H_{29}N_4O$ (M + H)$^+$ 329.2336, found 329.2344.

29. LC−MS (method 1): t_R = 5.19 min. HRMS (m/z) calcd for $C_{16}H_{17}N_4O$ (M + H)$^+$ 281.1397, found 281.1402.

30. [1H] NMR (400 MHz, DMSO-d_6) δ ppm 2.60 (s, 3 H), 2.74 (s, 3 H), 4.58 (d, J = 5.9 Hz, 2 H), 6.31 (d, J = 3.1 Hz, 1 H), 6.41 (m, 1 H), 7.12 (s, 1 H), 7.60 (m, 1 H), 8.38 (t, J = 5.9 Hz, 1 H), 8.52 (s, 1 H). LC−MS (method 1): t_R = 4.72 min. HRMS (m/z) calcd for $C_{14}H_{15}N_4O_2$ (M + H)$^+$ 279.1190, found 279.1189.

31. [1H] NMR (400 MHz, DMSO-d_6) δ ppm 2.71 (s, 3 H), 2.77 (s, 3 H), 7.10 (t, J = 7.4 Hz, 1 H), 7.20 (s, 1 H), 7.38 (t, J = 7.8 Hz, 2 H), 7.75 (d, J = 7.8 Hz, 2 H), 8.64 (s, 1 H), 10.19 (s, 1 H). LC−MS (method 1): t_R = 5.52 min. HRMS (m/z) calcd for $C_{15}H_{15}N_4O$ (M + H)$^+$ 267.1240, found 267.1241.

32. [1H] NMR (400 MHz, DMSO-d_6) δ ppm 2.29 (s, 3 H), 2.71 (s, 3 H), 2.77 (s, 3 H), 7.19 (m, 3 H), 7.63 (d, J = 8.6 Hz, 2 H), 8.62 (s, 1 H), 10.11 (s, 1 H). LC−MS (method 1): t_R = 5.82 min. HRMS (m/z) calcd for $C_{16}H_{17}N_4O$ (M + H)$^+$ 281.1397, found 281.1399.

33. [1H] NMR (400 MHz, DMSO-d_6) δ ppm 2.48 (s, 3 H), 2.68 (s, 3 H), 2.78 (s, 3 H), 7.02 (m, 1 H), 7.26 (m, 3 H), 8.34 (d, J = 8.2 Hz, 1 H), 8.64 (s, 1 H), 10.09 (s, 1 H). LC−MS (method 1): t_R = 5.73 min. HRMS (m/z) calcd for $C_{16}H_{17}N_4O$ (M + H)$^+$ 281.1397, found 281.1401.

34. [1H] NMR (400 MHz, DMSO-d_6) δ ppm 2.32 (s, 3 H), 2.69 (s, 3 H), 2.75 (s, 3 H), 6.90 (m, 1 H), 7.18 (m, 1 H), 7.24 (m, 1 H), 7.54 (m, 2 H), 8.60 (s, 1 H), 10.10 (s, 1 H). LC−MS (method 1): t_R = 5.84 min. HRMS (m/z) calcd for $C_{16}H_{17}N_4O$ (M + H)$^+$ 281.1397, found 281.1404.

35. [1H] NMR (400 MHz, DMSO-d_6) δ ppm 2.20 (s, 3 H), 2.25 (s, 3 H), 2.71 (s, 3 H), 2.77 (s, 3 H), 7.13 (d, J = 9.0 Hz, 1 H), 7.19 (s, 1 H), 7.49 (m, 2 H), 8.61 (s, 1 H), 10.04 (s, 1 H). LC−MS (method 1):t_R = 6.09 min. HRMS (m/z) calcd for $C_{17}H_{19}N_4O$ (M + H)$^+$ 295.1553, found 295.1555.

36. [1H] NMR (400 MHz, DMSO-d_6) δ ppm 2.26 (s, 3 H), 2.43 (s, 3 H), 2.66 (s, 3 H), 2.77 (s, 3 H), 7.02 (dd, J = 8.2, 2.0 Hz, 1 H), 7.09 (d, J = 2.0 Hz, 1 H), 7.20 (s, 1 H), 8.18 (d, J = 8.2 Hz, 1 H), 8.62 (s, 1 H), 10.01 (s, 1 H). LC−MS (method 1): t_R = 6.11 min. HRMS (m/z) calcd for $C_{17}H_{19}N_4O$ (M + H)$^+$ 295.1553, found 295.1561.

37. [1H] NMR (400 MHz, DMSO-d_6) δ ppm 2.03 (quin, J = 7.4 Hz, 2 H), 2.71 (s, 3 H), 2.77 (s, 3 H), 2.84 (t, J = 7.4 Hz, 2 H), 2.89 (t, J = 7.4 Hz, 2 H), 7.20 (m, 2 H), 7.46 (dd, J = 8.2, 1.6 Hz, 1 H), 7.66 (m, 1 H), 8.61 (s, 1 H), 10.11 (s, 1 H). LC−MS (method 1): t_R = 6.33 min. HRMS (m/z) calcd for $C_{18}H_{19}N_4O$ (M + H)$^+$ 307.1553, found 307.1560.

38. [1H] NMR (400 MHz, DMSO-d_6) δ ppm 1.18 (t, J = 7.6 Hz, 3 H), 2.59 (q, J = 7.4 Hz, 2 H), 2.70 (s, 3 H), 2.76 (s, 3 H), 7.20 (m, 3 H), 7.64 (d, J = 8.2 Hz, 2 H), 8.61 (s, 1 H), 10.10 (s, 1 H). LC−MS (method 1): t_R = 6.23 min. HRMS (m/z) calcd for $C_{17}H_{19}N_4O$ (M + H)$^+$ 295.1553, found 295.1558.

39. [1H] NMR (400 MHz, DMSO-d_6) δ ppm 1.29 (s, 9 H), 2.70 (s, 3 H), 2.77 (s, 3 H), 7.20 (s, 1 H), 7.39 (d, J = 9.0 Hz, 2 H), 7.64 (d, J = 8.6 Hz, 2 H), 8.62 (s, 1 H), 10.11 (s, 1 H). LC−MS (method 1): t_R = 6.75 min. HRMS (m/z) calcd for $C_{19}H_{23}N_4O$ (M + H)$^+$ 323.1866, found 323.1875.

40. [1H] NMR (400 MHz, DMSO-d_6) δ ppm 2.70 (s, 3 H), 2.76 (s, 3 H), 4.10 (s, 1 H), 7.19 (s, 1 H), 7.47 (d, J = 8.6 Hz, 2 H), 7.76 (d, J = 8.6 Hz, 2 H), 8.64 (s, 1 H), 10.29 (s, 1 H). [13C] NMR (101 MHz, DMSO-d_6) δ ppm 16.5, 24.4, 79.8, 83.5, 100.5, 103.7, 116.2, 118.9, 132.6, 139.3, 145.3, 145.3, 147.6, 159.8, 162.2. [13C] NMR (101 MHz, DMSO-d_6, 100 °C) δ ppm 15.6, 23.7, 78.6, 83.1, 103.5, 109.9, 115.9, 118.6, 131.9, 138.9, 144.7, 144.8, 147.0, 159.2, 161.4. LC−MS

(method 1): t_R = 5.78 min. HRMS (m/z) calcd for $C_{17}H_{15}N_4O$ (M + H)$^+$ 291.1240, found 291.1245.

41. [1H] NMR (400 MHz, DMSO-d_6) δ ppm 2.72 (s, 3 H), 2.78 (s, 3 H), 7.23 (s, 1 H), 7.74 (d, J = 8.6 Hz, 2 H), 7.98 (d, J = 8.6 Hz, 2 H), 8.68 (m, 1 H), 10.45 (m, 1 H). LC−MS (method 1): t_R = 6.43 min. HRMS (m/z) calcd for $C_{16}H_{14}F_3N_4O$ (M + H)$^+$ 335.1114, found 335.1116.

42. [1H] NMR (400 MHz, DMSO-d_6) δ ppm 2.69 (s, 3 H), 2.75 (s, 3 H), 7.18 (s, 1 H), 7.43 (m, 1 H), 7.59 (t, J = 7.9 Hz, 1 H), 7.85 (m, 1 H), 8.30 (t, J = 2.1 Hz, 1 H), 8.63 (s, 1 H), 10.35 (s, 1 H). LC−MS (method 1): t_R = 6.36 min. HRMS (m/z) calcd for $C_{16}H_{14}F_3N_4O$ (M + H)$^+$ 335.1114, found 335.1118.

43. [1H] NMR (400 MHz, DMSO-d_6) δ ppm 2.71 (s, 3 H), 2.77 (s, 3 H), 7.21 (s, 1 H), 7.56 (d, J = 8.6 Hz, 2 H), 7.74 (d, J = 9.0 Hz, 2 H), 8.65 (s, 1 H), 10.24 (s, 1 H). LC−MS (method 1): t_R = 6.21 min. HRMS (m/z) calcd for $C_{15}H_{14}BrN_4O$ (M + H)$^+$ 345.0346, found 345.0349.

44. [1H] NMR (400 MHz, DMSO-d_6) δ ppm 2.71 (s, 3 H), 2.77 (s, 3 H), 7.21 (s, 1 H), 7.65 (m, 2 H), 8.20 (d, J = 2.3 Hz, 1 H), 8.66 (s, 1 H), 10.30 (s, 1 H). LC−MS (method 1): t_R = 6.46 min. HRMS (m/z) calcd for $C_{15}H_{13}Cl_2N_4O$ (M + H)$^+$ 335.0461, found 335.0463.

45. LC−MS (method 1): t_R = 6.72 min. HRMS (m/z) calcd for $C_{15}H_{13}Cl_2N_4O$ (M + H)$^+$ 335.0461, found 335.0467.

46. [1H] NMR (400 MHz, DMSO-d_6) δ ppm 2.74 (s, 3 H), 2.79 (s, 3 H), 7.28 (s, 1 H), 8.15 (d, J = 6.3 Hz, 2 H), 8.69 (d, J = 6.3 Hz, 2 H), 8.77 (s, 1 H), 10.94 (s, 1 H). LC−MS (method 1): t_R = 3.33 min. HRMS (m/z) calcd for $C_{14}H_{14}N_5O$ (M + H)$^+$ 268.1193, found 268.1198.

47. [1H] NMR (400 MHz, DMSO-d_6) δ ppm 2.73 (s, 3 H), 2.78 (s, 3 H), 3.19 (s, 3 H), 7.23 (s, 1 H), 7.92 (m, 2 H), 8.00 (m, 2 H), 8.69 (d, J = 2.0 Hz, 1 H), 10.52 (d, J = 0.8 Hz, 1 H. LC−MS (method 1): t_R = 4.76 min. HRMS (m/z) calcd for $C_{16}H_{17}N_4O_3S$ (M + H)$^+$ 345.1016, found 345.1021.

48. [1H] NMR (400 MHz, DMSO-d_6) δ ppm 2.72 (s, 3 H), 2.77 (s, 3 H), 7.22 (s, 1 H), 7.84 (d, J = 8.7 Hz, 2 H), 7.96 (d, J = 8.7 Hz, 2 H), 8.68 (s, 1 H), 10.50 (s, 1 H). LC−MS (method 1): t_R = 5.44 min. HRMS (m/z) calcd for $C_{16}H_{15}N_5O$ (M + H)$^+$ 292.1193, found 292.1193.

49. [1H] NMR (400 MHz, DMSO-d_6) δ ppm 2.72 (s, 3 H), 2.77 (s, 3 H), 7.21 (s, 1 H), 7.57 (m, 2 H), 8.02 (m, 1 H), 8.28 (t, J = 2.0 Hz, 1 H), 8.66 (s, 1 H), 10.36 (s, 1 H). LC−MS (method 1): t_R = 5.47 min. HRMS (m/z) calcd for $C_{16}H_{14}N_5O$ (M + H)$^+$ 292.1193, found 292.1200.

50. LC−MS (method 1): t_R = 5.25 min. HRMS (m/z) calcd for $C_{17}H_{14}N_4O$ (M + H)$^+$ 291.1245, found 291.1240.

51. [1H] NMR (400 MHz, DMSO-d_6) δ ppm 2.61 (s, 3 H), 2.72 (s, 3 H), 2.78 (s, 3 H), 7.21 (s, 1 H), 7.54 (t, J = 7.8 Hz, 1 H), 7.71 (dt, J = 7.7, 1.3 Hz, 1 H), 7.95 (m, 1 H), 8.35 (t, J = 2.0 Hz, 1 H), 8.66 (s, 1 H), 10.30 (s, 1 H). LC−MS (method 1): t_R = 5.27 min. HRMS (m/z) calcd for $C_{17}H_{17}N_4O_2$ (M + H)$^+$ 309.1346, found 309.1349.

52. [1H] NMR (400 MHz, DMSO-d_6) δ ppm 2.04 (s, 3 H), 2.71 (s, 3 H), 2.77 (s, 3 H), 7.20 (s, 1 H), 7.58 (m, 2 H), 7.66 (m, 2 H), 8.62 (s, 1 H), 9.92 (s, 1 H), 10.10 (s, 1 H). LC−MS (method 1): t_R = 4.39 min. HRMS (m/z) calcd for $C_{17}H_{18}N_5O_2$ (M + H)$^+$ 324.1455, found 324.1459.

53. [1H] NMR (400 MHz, DMSO-d_6) δ ppm 2.08 (s, 3 H), 2.69 (s, 3 H), 2.77 (s, 3 H), 7.12 (m, 1 H), 7.19 (s, 1 H), 7.27 (m, 2 H), 8.18 (m, 1 H), 8.63 (s, 1 H), 9.74 (s, 1 H), 9.94 (s, 1 H. LC−MS (method 1): t_R = 4.17 min. HRMS (m/z) calcd for $C_{17}H_{18}N_5O_2$ (M + H)$^+$ 324.1455, found 324.1461.

54. [1H] NMR (400 MHz, DMSO-d_6) δ ppm 2.70 (s, 3 H), 2.77 (s, 3 H), 3.76 (s, 3 H), 6.96 (d, J = 9.0 Hz, 2 H), 7.19 (m, 1 H), 7.66 (d, J = 9.0 Hz, 2 H), 8.62 (s, 1 H), 10.03 (s, 1 H). LC−MS (method 1): t_R = 5.33 min. HRMS (m/z) calcd for $C_{16}H_{17}N_4O_2$ (M + H)$^+$ 297.1346, found 297.1352.

55. [1H] NMR (400 MHz, DMSO-d_6) δ ppm 2.71 (s, 3 H), 2.77 (s, 3 H), 3.65 (s, 3 H), 3.81 (s, 6 H), 7.09 (m, 2 H), 7.19 (s, 1 H), 8.61 (s, 1 H), 10.04 (d, J = 1.2 Hz, 1 H). LC−MS (method 1): t_R = 5.24 min. HRMS (m/z) calcd for $C_{18}H_{21}N_4O_4$ (M + H)$^+$ 357.1557, found 357.1564.

56. [1H] NMR (400 MHz, DMSO-d_6) δ ppm 2.70 (s, 3 H), 2.77 (s, 3 H), 3.75 (s, 3 H), 3.79 (s, 3 H), 6.96 (d, J = 8.6 Hz, 1 H), 7.18

(m, 2 H), 7.49 (d, J = 2.2 Hz, 1 H), 8.61 (s, 1 H), 10.01 (s, 1 H). LC−MS (method 1): t_R = 5.03 min. HRMS (m/z) calcd for $C_{17}H_{19}N_4O_3$ (M + H)$^+$ 327.1452, found 327.1456.

57. ^{1}H NMR (400 MHz, DMSO-d_6) δ ppm 2.70 (s, 3 H), 2.77 (s, 3 H), 6.02 (s, 2 H), 6.92 (d, J = 8.2 Hz, 1 H), 7.08 (dd, J = 8.4, 2.2 Hz, 1 H), 7.19 (s, 1 H), 7.51 (d, J = 2.3 Hz, 1 H), 8.61 (s, 1 H), 10.07 (s, 1 H). LC−MS (method 1): t_R = 5.33 min. HRMS (m/z) calcd for $C_{16}H_{15}N_4O_3$ (M + H)$^+$ 311.1139, found 311.1142

58. ^{1}H NMR (400 MHz, DMSO-d_6) δ ppm 2.69 (s, 3 H), 2.76 (s, 3 H), 4.24 (m, 4 H), 6.85 (d, J = 8.6 Hz, 1 H), 7.05 (m, 1 H), 7.18 (s, 1 H), 7.43 (d, J = 2.7 Hz, 1 H), 8.60 (s, 1 H), 10.00 (s, 1 H). LC−MS (method 1): t_R = 5.30 min. HRMS (m/z) calcd for $C_{17}H_{17}N_4O_2$ (M + H)$^+$ 325.1295, found 325.1299.

59. ^{1}H NMR (400 MHz, DMSO-d_6) δ ppm 2.71 (s, 3 H), 2.77 (s, 3 H), 3.83 (s, 3 H), 7.18 (m, 2 H), 7.40 (m, 1 H), 7.79 (dd, J = 13.5, 2.5 Hz, 1 H), 8.63 (s, 1 H), 10.11 (s, 1 H). LC−MS (method 1): t_R = 5.52 min. HRMS (m/z) calcd for $C_{16}H_{16}FN_4O_2$ (M + H)$^+$ 315.1252, found 315.1257.

60. ^{1}H NMR (400 MHz, DMSO-d_6) δ ppm 2.71 (s, 3 H), 2.77 (s, 3 H), 3.86 (s, 3 H), 7.17 (d, J = 9.0 Hz, 1 H), 7.20 (s, 1 H), 7.59 (dd, J = 8.6, 2.7 Hz, 1 H), 7.97 (d, J = 2.3 Hz, 1 H), 8.63 (s, 1 H), 10.08 (s, 1 H). LC−MS (method 1): t_R = 5.79 min. HRMS (m/z) calcd for $C_{16}H_{16}ClN_4O_2$ (M + H)$^+$ 331.0956, found 331.0962.

61. LC−MS (method 1): t_R = 3.72. LC−MS (m/z) calcd for $C_{13}H_{19}N_4O_2$(M + H)$^+$ 263.2, found 263.1. LC−MS (m/z) calcd for $C_{26}H_{36}N_8NaO_4$ (2M + Na)$^+$ 547.3, found 547.3.

62. ^{1}H NMR (400 MHz, DMSO-d_6) δ ppm 2.30 (s, 3 H), 2.79 (s, 3 H), 7.20 (d, J = 8.4 Hz, 2 H), 7.49 (s, 1 H), 7.65 (m, 5 H), 8.13 (m, 2 H), 8.65 (s, 1 H), 10.20 (s, 1 H). LC−MS (method 1): t_R = 6.59. HRMS (m/z) calcd for $C_{21}H_{19}N_4O$ (M + H)$^+$ 343.1553, found 343.1560.

63. ^{1}H NMR (400 MHz, DMSO-d_6) δ ppm 2.79 (s, 3 H), 3.76 (s, 3 H), 6.97 (d, J = 9.0 Hz, 2 H), 7.48 (s, 1 H), 7.65 (m, 5 H), 8.14 (dd, J = 7.8, 2.0 Hz, 2 H), 8.64 (s, 1 H), 10.12 (s, 1 H). LC−MS (method 1): t_R = 6.17.

64. ^{1}H NMR (400 MHz, DMSO-d_6) δ ppm 2.81 (s, 3 H), 7.51 (s, 1 H), 7.67 (m, 5 H), 8.13 (m, 2 H), 8.23 (d, J = 2.7 Hz, 1 H), 8.69 (s, 1 H), 10.40 (s, 1 H). LC−MS (method 1): t_R = 7.21 min. HRMS (m/z) calcd for $C_{20}H_{15}Cl_2N_4O$ (M + H)$^+$ 397.0617, found 397.0628.

65. ^{1}H NMR (400 MHz, DMSO-d_6) δ ppm 2.89 (s, 3 H), 7.65 (m, 5 H), 7.97 (s, 1 H), 8.22 (d, J = 2.7 Hz, 1 H), 8.35 (dd, J = 7.6, 2.2 Hz, 2 H), 8.75 (s, 1 H), 10.36 (s, 1 H). LC−MS (method 1): t_R = 7.26.HRMS (m/z) calcd for $C_{20}H_{15}Cl_2N_4O$ (M + H)$^+$ 397.0617, found 397.0622.

66. ^{1}H NMR (400 MHz, DMSO-d_6) δ ppm 2.53 (s, 3 H), 2.73 (s, 3 H), 7.17 (m, 7 H), 7.52 (m, 1 H), 7.62 (dd, J = 7.6, 1.8 Hz, 1 H), 8.60 (s, 1 H), 8.64 (m, 1 H), 10.90 (s, 1 H). LC−MS (method 1): t_R = 6.59.HRMS (m/z) calcd for $C_{21}H_{19}N_4OS$ (M + H)$^+$ 375.1274, found 375.1284.

67. LC−MS (method 3): t_R = 2.76 min. HRMS (m/z) calcd for $C_{23}H_{18}F_3N_4OS$ (M + H)$^+$ 455.1148, found 455.1161.

68. ^{1}H NMR (400 MHz, DMSO-d_6) δ ppm 2.62 (s, 3 H), 7.17 (m, 4 H), 7.26 (m, 2 H), 7.43 (s, 1 H), 7.54 (m, 1 H), 7.63 (m, 4 H), 8.10 (dd, J = 7.8, 2.0 Hz, 2 H), 8.67 (m, 2 H), 11.01 (s, 1 H). LC−MS (method 1): t_R = 7.28 min. HRMS (m/z) calcd for $C_{26}H_{21}N_4OS$ (M + H)$^+$ 437.1431, found 437.1441.

69. LC−MS (method 3): t_R = 2.64 min. HRMS (m/z) calcd for $C_{20}H_{19}F_2N_4O$ (M + H)$^+$ 369.1521, found 369.1529.

70. ^{1}H NMR (400 MHz, DMSO-d_6) δ ppm 2.04 (m, 2 H), 2.87 (m, 7 H), 7.24 (m, 1 H), 7.44 (m, 1 H), 7.67 (m, 4 H), 7.95 (s, 1 H), 8.33 (m, 2 H), 8.70 (s, 1 H), 10.16 (br s, 1 H). LC−MS (method 1): t_R = 7.03.HRMS (m/z) calcd for $C_{23}H_{21}N_4O$ (M + H)$^+$ 369.1710, found 369.1716.

71. LC−MS (method 3): t_R = 2.48 min. HRMS (m/z) calcd for $C_{17}H_{21}F_2N_4O$ (M + H)$^+$ 335.1678, found 335.1684.

72. LC−MS (method 2): t_R = 2.47 min. HRMS (m/z) calcd for $C_{17}H_{17}F_2N_4O$ (M + H)$^+$ 331.1365, found 331.1371.

73. ^{1}H NMR (400 MHz, DMSO-d_6) δ ppm 1.20 (t, J = 7.6 Hz, 3 H), 2.61 (q, J = 7.5 Hz, 2 H), 2.89 (s, 3 H), 7.25 (d, J = 8.4 Hz, 2 H), 7.68 (m, 5 H), 7.96 (s, 1 H), 8.33 (m, 2 H), 8.70 (s, 1 H), 10.17

(s, 1 H). LC−MS (method 1): t_R = 6.91 min. HRMS (m/z) calcd for $C_{20}H_{19}F_2N_4O$ (M + H)$^+$ 369.1521, found 369.1529.

ASSOCIATED CONTENT

ⓢ Supporting Information

Stereochemical prediction of relative sterechemistry of **27** and **28** and their NMR spectra. This material is available free of charge via the Internet at http://pubs.acs.org.

AUTHOR INFORMATION

Corresponding Author
*Phone: 301-217-9198. Fax: 301-217-5736. E-mail: maruganj@mail.nih.gov.

Notes
The authors declare no competing financial interest.

ACKNOWLEDGMENTS

ABBREVIATIONS USED

GCase, glucocerebrosidase; GC, glucocerebroside; ERT, enzymatic replacement therapy; SRT, substrate replacement therapy; ER, endoplasmic reticulum; NN-DNJ, N-(n-nonyl)-deoxynojirimycin; wt, wild type; NCGC, NIH Chemical Genomics Center; IC$_{50}$, half-maximal inhibitory concentration; AC$_{50}$, half-maximal activation concentration; 4MU-Glc, 4-methylumbelliferyl β-D-glucopyranoside; 4MU, 4-methylumbelliferone; HTS, high throughput screening; SAR, structure−activity relationship; MST, microscale thermophoresis; HPLC, high performance liquid chromatography; LC−MS, liquid chromatography−mass spectrometry; ADME, absorption, distribution, metabolism, elimination

REFERENCES

(1) Beutler, E.; Grabowski, G. A. Gaucher Disease. In *The Metabolic and Molecular Bases of Inherited Disease*, 8th ed.; Scriver, C. R., Beaudet, A. L., Sly, W. S., Valle, D., Eds.; McGraw-Hill: New York, 2001; pp 3635−3668.

(2) Germain, D. P. Gaucher's disease: a paradigm for interventional genetics. *Clin. Genet.* **2004**, *65*, 77−86.

(3) Grabowski, G. A. Gaucher disease. Enzymology, genetics, and treatment. *Adv. Hum. Genet.* **1993**, *21*, 377−441.

(4) Beutler, E.; Nguyen, N. J.; Henneberger, M. W.; Smolec, J. M.; McPherson, R. A.; West, C.; Gelbart, T. Gaucher disease: gene frequencies in the Ashkenazi Jewish population. *Am. J. Hum. Genet.* **1993**, *52*, 85−88.

(5) Beck, M. New therapeutic options for lysosomal storage disorders: enzyme replacement, small molecules and gene therapy. *Hum. Genet.* **2007**, *121*, 1−22.

(6) Grabowski, G. A. Phenotype, diagnosis, and treatment of Gaucher's disease. *Lancet* **2008**, *42*, 1263−1271 . Also see http://www.cerezyme.com.

(7) Beutler, E. Lysosomal storage diseases: natural history and ethical and economic aspects. *Mol. Genet. Metab.* **2006**, *25*, 147−151.

(8) Pastores, G. M.; Giraldo, P.; Cherin, P.; Mehta, A. Goal-oriented therapy with miglustat in Gaucher disease. *Curr. Med. Res. Opin.* **2009**, *25*, 23−37 . Also see http://www.zavesca.com/patient-home.asp.

(9) Futerman1, A. H.; Sussman, J. L.; Horowitz, M.; Silman, I.; Zimran, A. New directions in the treatment of Gaucher disease. *Trends Pharmacol. Sci.* 2004, 25, 147−151.

(10) Schiffmann, R.; Fitzgibbon, E. J.; Harris, C.; DeVile, C; Davies, E. H.; et al. Randomized, controlled trial of miglustat in Gaucher's disease type 3. *Ann. Neurol.* 2008, 64, 514−522.

(11) Montalvo, A. L.; Cariati, R.; Deganuto, M.; Guerci, V.; Garcia, R.; Ciana, G.; Bembi, B.; Pittis, M. G. Glycogenosis type II: identification and expression of three novel mutations in the acid alpha-glucosidase gene causing the infantile form of the disease. *Mol. Genet. Metab.* 2004, 81, 203−208.

(12) Hermans, M. M.; van Leenen, D.; Kroos, M. A.; Beesley, C. E.; Van der Ploeg, A. T.; Sakuraba, H.; Wevers, R.; Kleijer, W.; Michelakakis, H.; Kirk, E. P.; Fletcher, J.; Bosshard, N.; Basel-Vanagaite, L.; Besley, G.; Reuser, A. J. Twenty-two novel mutations in the lysosomal alpha-glucosidase gene (GAA) underscore the genotype−phenotype correlation in glycogen storage disease type II. *Hum. Mutat.* 2004, 23, 47−56.

(13) Reuser, A. J.; Kroos, M.; Willemsen, R.; Swallow, D.; Tager, J. M.; Galjaard, H. J. Clinical diversity in glycogenosis type II. Biosynthesis and in situ localization of acid alpha-glucosidase in mutant fibroblasts. *Clin. Invest.* 1987, 79, 1689−1699.

(14) Reuser, A. J.; Kroos, M.; Oude Elferink, R. P.; Tager, J. M. Defects in synthesis, phosphorylation, and maturation of acid alphaglucosidase in glycogenosis type II. *J. Biol. Chem.* 1985, 260, 8336−8341.

(15) Schmitz, M.; Alfalah, M.; Aerts, J. M. F. G.; Naim, H. Y.; Zimmer, K.-P. Impaired trafficking of mutants of lysosomal glucocerebrosidase in Gaucher's disease. *Int. J. Biochem. Cell Biol.* 2005, 37, 2310−2320.

(16) Ron, I.; Horowitz, M. ER retention and degradation as the molecular basis underlying Gaucher disease heterogeneity. *Hum. Mol. Genet.* 2005, 14, 2387−2398.

(17) Fan, J.-Q. A contradictory treatment for lysosomal storage disorders: inhibitors enhance mutant enzyme activity. *Trends Pharmacol. Sci.* 2003, 24, 355−360.

(18) Morello, J. P.; Petäjä-Repo, U. E.; Bichet, D. G.; Bouvier, M. Pharmacological chaperones: a new twist on receptor folding. *Trends Pharmacol. Sci.* 2000, 21, 466−469.

(19) Sawkar, A. R.; Schmitz, M. S.; Zimmer, K.-P.; Reczek, D.; Edmunds, T.; Balch, W. E.; Kelly, J. W. Chemical chaperones and permissive temperatures alter the cellular localization of Gaucher disease associated glucocerebrosidase variants. *ACS Chem. Biol.* 2006, 1, 235−251.

(20) Wei, R. R.; Hughes, H.; Boucher, S.; Bird, J. J.; Guziewicz, N.; Van Patten, S. M.; Qiu, H.; Qun Pan, C.; Edmunds, T. X-ray and biochemical analysis of N370S mutant human acid β-glucosidase. *J. Biol. Chem.* 2011, 286, 299−308.

(21) Benito, J. M.; Fernández, J. M.; Mellet, C. O. Pharmacological chaperone therapy for Gaucher disease: a patent review. *Expert Opin. Ther. Pat.* 2011, 21, 885−903.

(22) Fan, J.-Q.; Ishii, S. Active-site-specific chaperone therapy for Fabry disease. Yin and Yang of enzyme inhibitors. *FEBS J.* 2007, 274, 4962−4971.

(23) Sawkar, A. R.; Cheng, W.-C.; Beutler, E.; Wong, C.-H.; Balch, W. E.; Kelly, J. W. Chemical chaperones increase the cellular activity of N370S β-glucosidase: a therapeutic strategy for Gaucher disease. *Proc. Natl. Acad. Sci. U.S.A.* 2002, 99, 15428−15433.

(24) Yu, Z.; Sawkar, A. R.; Whalen, L. J.; Wong, C.-H.; Kelly, J. W. Isofagomine- and 2,5-anhydro-2,5-imino-D-glucitol-based glucocerebrosidase pharmacological chaperones for Gaucher disease intervention. *J. Med. Chem.* 2007, 50, 94−100.

(25) Zhu, X.; Sheth, K. A.; Li, S.; Chang, H.-H.; Fan, J.-Q. Rational design and synthesis of highly potent β-glucocerebrosidase inhibitors. *Angew. Chem., Int. Ed.* 2005, 44, 7450−7453.

(26) Aguilar, M.; Gloster, T. M.; Garcia-Moreno, M. I.; Mellet, C. O.; Davies, G. J.; Llebaria, A.; Casas, J.; Egido-Gabás, M.; Fernandez, J. M. G. Molecular basis for beta-glucosidase inhibition by ring-modified calystegine analogues. *ChemBioChem* 2008, 9, 2612−2618.

(27) Egido-Gabás, M.; Canals, D.; Casas, J.; Llebaria, A.; Delgado, A. Aminocyclitols as pharmacological chaperones for glucocerebrosidase, a defective enzyme in Gaucher disease. *ChemMedChem* 2007, 2, 992−994.

(28) Compain, P; Martin, O. R.; Boucheron, C.; Godin, G.; Yu, L.; Ikeda, K.; Asano, N. Design and synthesis of highly potent and selective pharmacological chaperones for the treatment of Gaucher's disease. *ChemBioChem* 2006, 7, 1356−1359.

(29) Steet, R. A.; Chung, S.; Wustman, B.; Powe, A.; Do, H.; Kornfeld, S. A. The iminosugar isofagomine increases the activity of N370S mutant acid beta-glucosidase in Gaucher fibroblasts by several mechanisms. *Proc. Natl. Acad. Sci. U.S.A.* 2006, 103, 13813−13818.

(30) Amicus Therapeutics. Amicus Therapeutics Announces Preliminary Results of Phase 2 Study with Plicera for Gaucher Disease. http://ir.amicustherapeutics.com/ReleaseDetail.cfm?ReleaseID=413437.

(31) Zheng, W.; Padia, J.; Urban, D. J.; Jadhav, A.; Goker-Alpan, O.; Simeonov, A.; Goldin, E.; Auld, D.; LaMarca, M. E.; Inglese, J.; Austin, C. P.; Sidransky, E. Three classes of glucocerebrosidase inhibitors identified by quantitative high-throughput screening are chaperone leads for Gaucher disease. *Proc. Natl. Acad. Sci. U.S.A.* 2007, 104, 13192−13197.

(32) Huang, W.; Zheng, W.; Urban, D. J.; Inglese, J.; Sidransky, E.; Austin, C. P.; Thomas, C. J. N4-Phenyl modifications of N2-(2-hydroxyl)ethyl-6-(pyrrolidin-1-yl)-1,3,5-triazine-2,4-diamines enhance glucocerebrosidase inhibition by small molecules with potential as chemical chaperones for Gaucher disease. *Bioorg. Med. Chem. Lett.* 2007, 17, 5783−5789.

(33) Tropak, M. B.; Kornhaber, G. J.; Rigat, B. A.; Maegawa, G. H.; Buttner, J. D.; Blanchard, J. E.; Murphy, C.; Tuske, S. J.; Coales, S. J.; Hamura, Y.; Brown, E. D.; Mahuran, D. J. Identification of pharmacological chaperones for Gaucher disease and characterization of their effects on beta-glucocerebrosidase by hydrogen/deuterium exchange mass spectrometry. *ChemoBioChem* 2008, 9, 2650−2662.

(34) Goldin, E.; Zheng, W.; Motabar, O.; Southall, N.; Choi, J. H.; Marugan, J. J.; Austin, C. P.; Sidransky, E. High throughput screening for small molecule therapy for Gaucher disease using patient tissue as the source of mutant glucocerberosidase. *PLoS One* 2012, 7, e29861.

(35) Marugan, J. J.; Zheng, W.; Motabar, O.; Southall, N.; Goldin, E.; Westbroek, W.; Stubblefield, B. K.; Sidransky, E.; Aungst, R. A.; Lea, W. A.; Simeonov, A.; Leister, W.; Austin, C. P. Evaluation of quinazoline analogues as glucocerebrosidase inhibitors with chaperone activity. *J. Med. Chem.* 2010, 54, 1033−1058.

(36) Marugan, J. J.; Huang, W.; Motabar, O.; Zheng, W.; Xiao, J.; Patnaik, S.; Southall, N.; Westbroek, W.; Lea, W. A.; Simeonov, A.; Goldin, E.; DeBernardi, M. A.; Sidransky, E. Non-iminosugar glucocerebrosidase small molecule chaperones. *Med. Chem. Commun.* 2012, 3, 56−60.

(37) Kuriyama, C.; Kamiyama, C.; Ikeda, K.; Sanae, F.; Kato, A.; Adachi, I.; Imahori, T.; Takahata, H.; Okamoto, T.; Asano, N. In vitro inhibition of glycogen-degrading enzymes and glycosidases by six-membered sugar mimics and their evaluation in cell cultures. *Bioorg. Med. Chem.* 2008, 16, 7330−7336.

(38) John, M.; Wendeler, M.; Heller, M.; Sandhoff, K.; Kessler, H. Characterization of human saposins by NMR spectroscopy. *Biochemistry* 2006, 45, 5206−5216.

(39) (a) Lieberman, R. L. A Guided tour of the structural biology of Gaucher disease: acid-β-glucosidase and saposin C. *Enzyme Res.* 2011, DOI 10.4061/2011/973231. (b) Vaccaro, A. M.; Salvioli, R.; Barca, A.; Tatti, M.; Ciaffoni, F.; Maras, B.; Siciliano, R.; Zappacosta, F.; Amoresano, A.; Pucci, P. Structural analysis of saposin C and B. Complete localization of disulfide bridges. *J. Biol. Chem.* 1995, 270, 9953−9960.

(40) Urban, D. J.; Zheng, W.; Goker-Alpan, O.; Jadhav, A.; LaMarca, M. E.; Inglese, J.; Sidransky, E.; Austin, C. P. Optimization and validation of two miniaturized glucocerebrosidase enzyme assays for high-throughput screening. *Comb. Chem. High Throughput Screening* 2008, 11, 817−824.

(41) van Weely, S.; van den Berg, M.; Barranger, J. A.; Sa Miranda, M. C.; Tager, J. M.; Aerts, J. M. Role of pH in determining the cell-type-specific residual activity of glucocerebrosidase in type 1 Gaucher disease. *J. Clin. Invest.* **1993**, *91*, 1167−1175.

(42) The data from the primary screening and all the inhibitory curves of every final compound in all the described assays are available online (PubChem BioAssay numbers 2101, 2590, 2592, 2588, 2595, 2597, 2596, 2577, 2578, 2587, 2589, 2593).

(43) Sawkar, A. R.; D'Haeze, W.; Kelly, J. W. Therapeutic strategies to ameliorate lysosomal storage disorders: a focus on Gaucher disease. *Cell. Mol. Life Sci.* **2006**, *63*, 1179−1192.

(44) The original screening data that include the structures of all active, inactive, and inconclusive compounds with structural analysis are available online (PubChem BioAssay number 2101).

(45) Inglese, J.; Auld, D. S.; Jadhav, A.; Johnson, R. L.; Simeonov, A.; Yasgar, A.; Zheng, W.; Austin, C. P. Quantitative high-throughput screening: a titration-based approach that efficiently identifies biological activities in large chemical libraries. *Proc. Natl. Acad. Sci. U S A.* **2006**, *103*, 11473−11478.

(46) This has been observed with other chemical series of inhibitors toward GCase at the NCGC.

(47) Nitz, T. J.; Salzwedel, K.; Finnegan, C.; Wild, C.; Brunton, S.; Flanagan, S.; Montalbetti, C.; Coulter, T. S.; Kimber, M.; Magaraci, F.; Johnston, D. Alpha-Unsubstituted Arylmethyl Piperazine Pyrazolo[1,5-a]pyrimidine Amide Derivatives. WO 2008/134035, 2008.

(48) Huppatz, J. L. Systemic fungicides. The synthesis of pyrazolo-[1,5-a]pyrimidine analogues of carboxin. *Aust. J. Chem.* **1985**, *38*, 221−230.

(49) Hayashi, Y.; Zama, K.; Abe, E.; Okino, N.; Inoue, T.; Ohno, K.; Ito, M. A sensitive and reproducible fluorescent-based HPLC assay to measure the activity of acid as well as neutral β-glucocerebrosidases. *Anal. Biochem.* **2008**, *283*, 122−129.

(50) Schmitz, M.; Alfalah, M.; Aerts, J. M.; Naim, H. Y.; Zimmer, K. P. Impaired trafficking of mutants of lysosomal glucocerebrosidase in Gaucher's disease. *Int. J. Biochem. Cell Biol.* **2005**, *37*, 2310−2320.

(51) Lieberman, R. L.; Wustman, B. A.; Huertas, P.; Powe, A. C., Jr.; Pine, C. W.; Khanna, R.; Schlossmacher, M. G.; Ringe, D.; Petsko, G. A structure of acid beta-glucosidase with pharmacological chaperone provides insight into Gaucher disease. *Nat. Chem. Biol.* **2007**, *3*, 101−107.

(52) Stone, D. L.; Tayebi, N.; Orvisky, E.; Stubblefield, B.; Madike, V.; Sidransky, E. Glucocerebrosidase gene mutations in patients with type 2 Gaucher disease. *Hum. Mutat.* **2000**, *15*, 181−188.

(53) Jerabek-Willemsen, M.; Wienken, C. J.; Braun, D.; Baaske, P.; Duhr, S. Molecular interaction studies using microscale thermophoresis. *Assay Drug Dev. Technol.* **2011**, *9*, 342−353.

(54) This type of interaction cannot be easily detected by other methods, such as differential scanning fluorimetry (no change in protein T_m upon compound dilution, data not shown) or isothermal titration calorimetry (requires a remarkably higher amount of protein in order to obtain a detectable amount of heat).

(55) Marugan, J. J.; Zheng, W.; Motabar, O.; Southall, N.; Goldin, E.; Sidransky, E.; Aungst, R. A.; Liu, K.; Sadhukhan, S. K.; Austin, C. P. Evaluation of 2-thioxo-2,3,5,6,7,8-hexahydropyrimido[4,5-d]pyrimidin-4(1H)-one analogues as GAA activators. *Eur. J. Med. Chem.* **2010**, *45*, 1880−1897.